PERGAMON

Deep-Sea Research II 49 (2002) 363–401

DEEP-SEA RESEARCH
PART II

www.elsevier.com/locate/dsr2

Oceanic vertical exchange and new production: a comparison between models and observations

Anand Gnanadesikan[a,*], Richard D. Slater[a], Nicolas Gruber[b], Jorge L. Sarmiento[a]

[a] *AOS Program, Princeton University, P.O. Box CN710, Princeton, NJ 08544, USA*
[b] *Department of Geosciences, University of California, Los Angeles, CA, USA*

Accepted 22 June 2001

Abstract

This paper explores the relationship between large-scale vertical exchange and the cycling of biologically active nutrients within the ocean. It considers how the parameterization of vertical and lateral mixing effects estimates of new production (defined as the net uptake of phosphate). A baseline case is run with low vertical mixing in the pycnocline and a relatively low lateral diffusion coefficient. The magnitude of the diapycnal diffusion coefficient is then increased within the pycnocline, within the pycnocline of the Southern Ocean, and in the top 50 m, while the lateral diffusion coefficient is increased throughout the ocean. It is shown that it is possible to change lateral and vertical diffusion coefficients so as to preserve the structure of the pycnocline while changing the pathways of vertical exchange and hence the cycling of nutrients. Comparisons between the different models reveal that new production is very sensitive to the level of vertical mixing within the pycnocline, but only weakly sensitive to the level of lateral and upper ocean diffusion. The results are compared with two estimates of new production based on ocean color and the annual cycle of nutrients. On a global scale, the observational estimates are most consistent with the circulation produced with a low diffusion coefficient within the pycnocline, resulting in a new production of around 10 GtC yr^{-1}. On a regional level, however, large differences appear between observational and model based estimates. In the tropics, the models yield systematically higher levels of new production than the observational estimates. Evidence from the Eastern Equatorial Pacific suggests that this is due to both biases in the data used to generate the observational estimates and problems with the models. In the North Atlantic, the observational estimates vary more than the models, due in part to the methodology by which the nutrient-based climatology is constructed. In the North Pacific, the modelled values of new production are all much lower than the observational estimates, probably as a result of the failure to form intermediate

*Corresponding author.
E-mail addresses: gnana@splash.princeton.edu (A. Gnanadesikan), rdslater@splash.princeton.edu (R.D. Slater), jls@splash.princeton.edu (J.L. Sarmiento).

0967-0645/01/$ - see front matter
PII: S0967-0645(01)00107-2

water with the right properties. The results demonstrate the potential usefulness of new production for evaluating circulation models. © 2001 Published by Elsevier Science Ltd.

1. Introduction

Ocean biology is strongly controlled by ocean circulation. Most organic matter sinking out of the surface ocean is remineralized by bacterial processes, increasing the nutrient content of thermocline and abyssal waters. Productive ecosystems are largely found in regions where these waters are brought to the surface. The magnitude of biological productivity is thus closely linked to the magnitude of vertical exchange. This paper considers how the physical processes driving large-scale oceanic vertical exchange can affect biological productivity, and in turn whether observational estimates of biological productivity can be used to identify systematic weaknesses in ocean models.

The physics responsible for driving large-scale oceanic vertical exchange, in particular the thermohaline overturning circulation, has been the subject of much debate. In contrast with the wind-driven gyres, where the dynamics are relatively well understood and numerical models do a fairly good job at capturing the shape of density surfaces away from boundary regions, major questions remain about how the thermohaline overturning is driven. Two major driving mechanisms for energizing the thermohaline overturning circulation have been proposed: vertical mixing within the low-latitude pycnocline and Southern Ocean winds. A recent paper (Gnanadesikan, 1999a) developed a simple theory for this overturning (shown schematically in Fig. 1) that includes both these mechanisms, as well as a parameterization of the effects of mesoscale eddies.

The theory divides the ocean into a "light-water sphere" (analogous to the "Warmwasser-sphere" of Wust) and a "dense-water sphere". The scaling depth for the light-water sphere is the

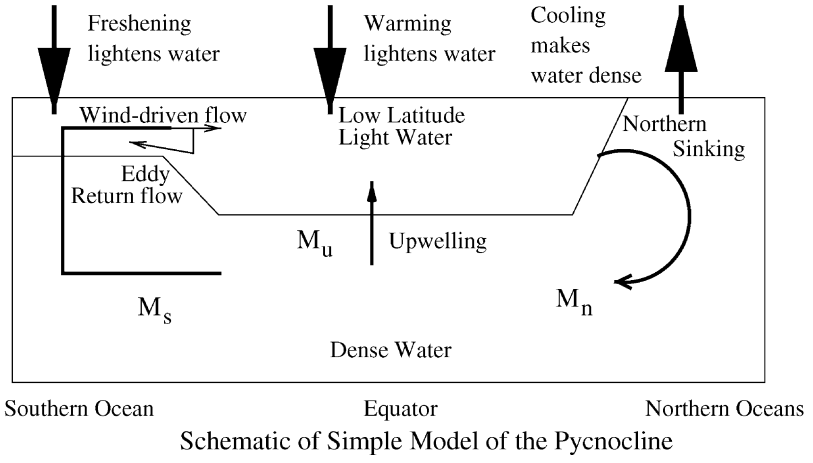

Fig. 1. Schematic of the ocean circulation proposed by Gnanadesikan (1999), showing the formation of abyssal water in the north and the upwelling of this water in either the low latitudes or the Southern Ocean.

pycnocline depth D. This is defined as

$$D = -\frac{\int_{-D}^{0} (\rho_{\max} - \rho) z \, dz}{\int_{-D}^{0} (\rho_{\max} - \rho) \, dz}, \tag{1}$$

where $\rho_{\max}$ is the maximum potential density within the water column, and ρ is the local density. If the density follows an exponential profile, D is then the e-folding depth of the density anomaly. If the density profile were to be characterized by a single density jump (as in layer models) at some depth Z, $D = Z/2$. The average pycnocline depth in the low-latitude ocean (averaged from 40S to 40N) is around 460 m.

Following numerous other authors (Bryan, 1987; Hughes and Weaver, 1994; Park and Bryan, 2000), Gnanadesikan (1999a) links the formation rate of dense abyssal water in the north (M_n) to the meridional pressure gradient, which goes as the square of the pycnocline depth D. The counterbalancing formation of light water can occur either in the low-latitude pycnocline as downward diffusion of heat is balanced by upwelling of cold abyssal water, or in the Southern Ocean as deep water is drawn to the surface by the winds, then freshened and warmed as it moves northward in the Ekman layer. The low-latitude upwelling flux is proposed to scale as

$$M_u = K_v A / D, \tag{2}$$

where A is the area of the low-latitude pycnocline, and K_v is the vertical diffusion coefficient.

The major difference between Gnanadesikan (1999a) and previous scaling theories is the inclusion of a flux of water from the abyssal Southern Ocean into the light-water sphere (M_s). This flux consists of two components, an Ekman upwelling flux (M_{ek}) and a compensating return flow associated with mesoscale eddies.

$$M_s = M_{ek} - A_I D L_x / L_y^s, \tag{3}$$

where M_{ek} is the northward Ekman flux at the latitude of the southern tip of South America, A_I is a lateral eddy diffusion coefficient that governs the residual mass flux associated with eddies as well as the along-isopycnal diffusion (Gent and McWilliams, 1990; Griffies, 1998), L_x is the circumference of the earth along a latitude circle in Drake Passage, and L_y^s is the north–south scale over which the pycnocline shallows in the Southern Ocean.

It is possible to obtain a realistic solution for D with different values of K_v and A_I. However, these different solutions will correspond to very different patterns of circulation and vertical exchange. If either K_v or A_I is large (or Southern Ocean winds are weak), the dominant pathway of transformation of abyssal waters into light water will occur within the low-latitude pycnocline. Conversely, if either K_v or A_I is small (or Southern Ocean winds are strong), the dominant pathway of transformation is within the Southern Ocean. Thus, by changing K_v and A_I together, it is possible to change the relative fraction of the Northern Hemisphere overturning supplied through these different pathways, while keeping the magnitude of the overturning and the large-scale density structure relatively constant.

There is still debate over the true value of K_v and A_I. While a considerable amount of work has been undertaken by physical oceanographers to estimate both of these coefficients in a large number of regions, much of the ocean remains unsampled. Recent observations, in particular the North Atlantic Tracer Release Experiment (NATRE, Ledwell et al., 1993, 1998), find low values of vertical mixing in the subtropical thermocline. These results are consistent with microstructure

measurements (Peters et al. (1988) below 100 m along the equator, Toole et al. (1994) in the NATRE region), which find values of vertical mixing around $0.1-0.2\ cm^2\ s^{-1}$. A number of oceanographers, however, have continued to argue that these low values do not properly represent the global average for the thermocline, and have postulated circulations driven by higher mixing along the boundaries (Marotzke, 1997). Huang (1999) argues that such high vertical mixing is necessary to stir down light water in low latitudes and "energize" the ocean circulation. Gibson (1999) also has argued that along the equator, turbulent mixing events may be extremely intermittent (Lilover et al., 1993), and so has been undersampled by microstructure profilers.

As pointed out by a number of authors, (Worthington, 1977; Wunsch et al., 1983; Gnanadesikan and Toggweiler, 1999) measurements of nutrient cycling can be used to put constraints on the large-scale vertical exchange. The last of these papers used regional estimates of biogenic silica production and export to place limits on the amount of upwelling at low latitudes, as well as on the amount of convection at high latitudes. Using an annual mean model of ocean circulation, it was argued that sufficiently low values of biogenic silica production were found only with low K_v, and with the Gent and McWilliams (1990) implementation of lateral diffusion, which suppresses Southern Ocean convection. These results supported the idea that the ocean is currently in a "low-mixing" regime where the effects of Southern Ocean winds are important. However, the results of Gnanadesikan and Toggweiler (1999) suffer from a number of weaknesses. The data used to constrain the models were largely taken from sediment traps that sample sparsely in space and in time and whose collection efficiency is not well established. Furthermore, the models had relatively low vertical resolution (12 levels) and did not include a seasonal cycle.

The present work looks at the cycle of phosphorus and carbon in a model with higher vertical resolution that includes seasonal cycling. It examines the following question—to what extent can models with different mixing parameterizations produce pycnocline structures that are similar while producing biogeochemical cycles that differ significantly?

2. Oceanic productivity

Before proceeding further, it is important to define exactly what is meant by new, export and primary production. When organic matter is produced as a result of photosynthesis, carbon, nitrogen, and phosphorus are taken up from the water column. The uptake is usually in a stoichiometric ratio of around 117 : 16 : 1 (Anderson and Sarmiento, 1995). Although there are organisms for which this is not the case (nitrogen fixers in low latitudes and phaeocystis in the Antarctic) the fact that dissolved nutrient ratios in the ocean are relatively close to these values indicates that the majority of production and dissolution is governed by these stoichiometric ratios. This fact allows us to model nitrogen and phosphorus relatively interchangeably.

In the classic paradigm for ocean ecosystems (Dugdale and Goering, 1967; Eppley and Peterson, 1979) the *net primary production* represents the total uptake of dissolved inorganic nutrients from the water. It represents the difference between the carbon fixed by photosynthesis and the carbon that is respired by phytoplankton. The *new production* is that portion of the primary production for which nitrate is the source of nitrogen. Ammonia produced by bacteria feeding on dissolved organic matter or by zooplankton feeding on phytoplankton accounts for the

great majority of the remainder of the nitrogen supply. The ratio between new and primary production is the *f-ratio* (Eppley and Peterson, 1979).

Because it is the preferred source of nitrogen for plankton, ammonia is generally consumed within the mixed layer. As a result, virtually all of the nitrogen that enters the mixed layer as a result of upwelling and convection does so in the form of nitrate. Because of this, the export of nitrogen of all forms is roughly equal to the new production. The form of export may be particulate matter that sinks relatively quickly, or dissolved organic matter that may have a half-life of months or years. In one-dimensional steady-state models the export ratio (the ratio of exported nitrogen to primary production) is equivalent to the f-ratio, so that some authors (including Laws et al., 2000) speak of an ef-ratio. It should be emphasized, however, that in regions where there is rapid advection, ammonia and dissolved organic nitrogen produced at one point may fuel production at a location tens to hundreds of kilometers away. It is possible for the production within a region to be completely fuelled by regenerated forms of nitrogen (or phosphorus) advected in laterally. The resulting ecosystem would have an f-ratio that is zero but a nonzero export ratio.

Different techniques estimate different parts of the production cycle, a fact that can impede comparison. General circulation models (as well as empirical techniques that utilize observations of surface nutrients) naturally estimate the new production. Satellites, on the other hand, estimate the total biomass, which in turn depends on the primary production, requiring an estimate of the f-ratio in order to obtain an estimate of new production. This paper uses a robust relationship that ties the f-ratio to temperature and primary production to bridge the gap between the two methods. More details of how this is done are given in the following section.

3. Methods

3.1. The physical models

We begin by describing the physical simulations done as part of this study. The model used is the Modular Ocean Model, Version 3 (Pacanowski and Griffies, 1999). The horizontal grid has a nominal resolution of 4° and is the same grid as was used in the GFDL coupled climate model in previous carbon cycle studies (Sarmiento et al., 1998). The topography is essentially identical to these runs, with the small difference that the Bering Straits are opened, allowing a throughflow of 0.8 Sv. The vertical grid has twice the resolution as the coupled model grid (24 instead of 12 levels). The topmost level is 25 m and the bottommost is 450 m thick.

A key difference between this model and previous incarnations of the Princeton Ocean Biogeochemical Model (Najjar et al., 1992; Murnane et al., 1999) is a more realistic inclusion of the effects of mesoscale eddies. In previous versions of the model, the subgrid scale mixing associated with these eddies was either purely horizontal or at least had a significant component in the horizontal direction. In this model, the discretization of isopycnal mixing developed by Griffies et al. (1998) is used. This allows us to reduce greatly the horizontal diffusion, which has been blamed for unrealistic diapycnal fluxes at ocean boundaries (Veronis, 1975) in previous model runs. Additionally, the so-called "Gent-McWilliams" parameterization of the advective effects of mesoscale eddies (Gent and McWilliams, 1990; Gent et al., 1995; Griffies, 1998) is

included. In addition to producing a more stratified ocean, this parameterization also acts to stabilize biological cycling schemes from instabilities driven by discretization errors on a Cartesian grid (Gnanadesikan, 1999c).

The physical forcing is a combination of diagnostic and applied fluxes. Applied fluxes of heat and fresh water were taken from the climatology of da Silva et al. (1994). These fluxes have biases (they do not sum to zero on a global scale). However, it is not clear how best to correct them since the imbalance may arise from regional biases. For this reason, a diagnostic flux calculated by restoring the temperature and salinity to observed values was applied over the uppermost box. The strength of the restoring used (a 30-day time constant applied over a 25-m thick box) is approximately one-half of that used in the studies of Toggweiler and Samuels (1993, 1998) and Gnanadesikan and Toggweiler (1999). Such restoring is often used in climate models, but the true physical meaning is frequently elusive. We would argue that the restoring should be thought of as a kind of data assimilation. The fluxes (particularly of fresh water) are poorly known, but temperature and salinity are relatively well known. Thus, by restoring the temperature and salinity to climatological averages (while applying a "first guess" heat flux), more realistic climatological heat, and water fluxes can be generated that are in agreement with the observed temperature and salinity distribution. Wind stresses were given by the climatology of Hellerman and Rosenstein (1983), as in previous runs of the POBM.

The basic set of model runs done as part of this study involved evaluating the sensitivity of the biological cycling of phosphate and carbon to changes in the vertical and lateral diffusivity. An initial matrix of four runs was made. These runs are denoted by the vertical diffusivity (KVLOW,KVHIGH) plus the lateral (along-isopycnal) diffusivity (AILOW,AIHIGH), so that KVLOW + AILOW is a run with low vertical and lateral diffusivity.

- KVLOW + AILOW: An initial run was made using values for lateral and vertical diffusivity within the upper ocean based on results from tracer release experiments (Ledwell et al., 1993, 1998) within the pycnocline in the Eastern Subtropical Atlantic. These experiments found a lateral (along-isopycnal) diffusivity of order 1000 $m^2\ s^{-1}$ and an explicit vertical diffusivity of 0.15 $cm^2\ s^{-1}$ within the pycnocline. However, higher diffusivities associated with wave breaking over rough topography have been found in other parts of the ocean (Polzin et al., 1997) and are required to close the mass and salt budget in many ocean basins (Whitehead and Worthington, 1982; Johnson et al., 1991). In order to account for these observations, we let K_v be a function of depth, increasing to 1.3 $cm^2\ s^{-1}$ with a hyperbolic tangent transition at 2500 m (solid line, Fig. 2). The deep value is exactly the same as in Bryan and Lewis (1979) and is similar to that suggested by Sjoberg and Stigebrandt (1992) based on estimates of tidal dissipation.
- KVHIGH + AIHIGH: A second run was made with a higher level of lateral mixing everywhere within the ocean, and a higher level of vertical mixing within the pycnocline. The physical justification for increasing the lateral mixing is based on the fact that the primary effects of this diffusion are found in regions where the isopycnals slope steeply (such as boundary currents and the Southern Ocean). Since such regions are prone to baroclinic instability, and are the regions where most of the eddy transport occurs, it has been argued (Held and Larichev, 1996; Visbeck et al., 1997) that the diffusion of isopycnal thickness should reflect the larger values of such regions rather than the lower values found in the relatively quiescent subtropical gyres. A value of 2000 $m^2\ s^{-1}$ was chosen to test the effect of increasing the lateral diffusivity. Such an

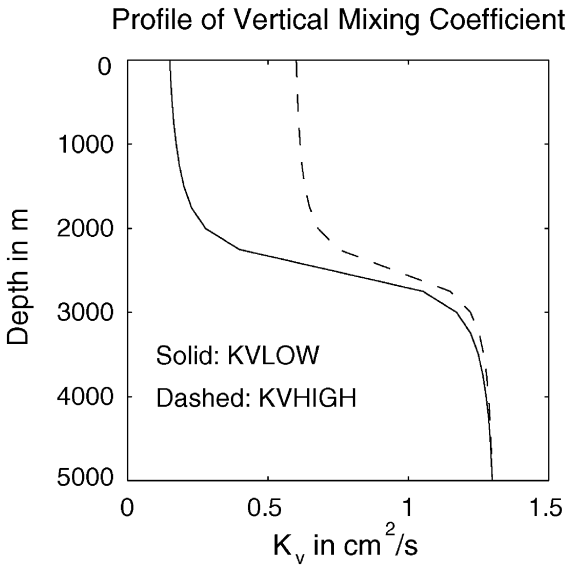

Fig. 2. Vertical diffusion coefficient K_v vs. depth for the KVLOW (solid) and KVHIGH (dashed) simulations.

increase in lateral diffusivity would be expected to cause a decrease in the depth of the pycnocline and magnitude of the Northern Hemisphere overturning (Gnanadesikan, 1999a). To counteract this effect, the vertical diffusion coefficient was increased to 0.6 $cm^2\ s^{-1}$ within the upper ocean while keeping the deep ocean at the same value of 1.3 $cm^2\ s^{-1}$ (dashed line, Fig. 2).

- KVHIGH + AILOW, KVLOW + AIHIGH: In order to isolate the effects of increasing vertical diffusion and increasing lateral diffusion, runs were made in which only one of the parameters was changed.

In order to evaluate where the additional mixing was important, two additional runs were made. The first (KVHISOUTH + AILOW) increased the vertical mixing only in the Southern Ocean. This run was motivated by recent observational work in the Southern Ocean (Polzin, 1999) that indicates that the level of internal wave activity is very high there. Theoretical formulations for K_v that reproduce the low values found in the low-latitude pycnocline predict extremely high values of mixing coefficient (of order 1 $cm^2\ is^{-1}$) at relatively shallow depths due to the high internal wave activity. In order to evaluate the importance of increasing the mixing in high southern latitudes, run KVHISOUTH was made in which the mixing coefficient was increased to 1.0 $cm^2\ s^{-1}$ south of 55S throughout the upper water column.

It might be supposed that differences between different models might result from the lack of resolution of a high-mixing surface layer. The GCM does mix convectively, but there is no explicit mixing due to winds, as is found in the real ocean (Price et al., 1986; Gnanadesikan and Weller, 1995). To test the effects of near-surface mixing, a final run (KVHIMIX + AILOW) was made in which the diffusivity between the top two boxes was increased to 50 $cm^2\ s^{-1}$. While this value is large in comparison with the thermocline, it is not unduly large for the surface layer

(Gnanadesikan and Weller, 1995; Price and Sundermeyer, 1999). Simply increasing the diffusion coefficient near the surface is a very crude approximation to what actually occurs in an oceanic mixed layer. However, in order to capture the dynamics that drive real ocean mixed layers, it would be necessary to consider diurnal cycling and synoptic variability of winds (Price et al., 1986; Price and Sundermeyer, 1999). Additionally, resolving the detailed structure of the surface mixing requires much higher resolution in the upper ocean. Given the lack of temporal resolution in the surface fluxes and vertical resolution in the model grid it did not seem appropriate to invest too much energy in running the model so as to resolve diurnal variations in mixing and Kelvin–Helmholtz instability driven by inertial oscillations. Instead, we concentrate on representing the primary effect of these unresolved physical processes, namely increasing the rate of mixing over the top 50 m or so of the water column.

3.2. Estimating new production using a circulation model

The first method used to estimate new production is to run the general circulation models described in Section 3.1 to estimate diagnostically the distribution and magnitude of biological production that would maintain the surface nutrient distribution given the model transport and depth-dependence of remineralization. This approach was taken during the OCMIP-2 modelling exercise (Najjar and Orr, 1998) upon which these simulations are based. Such a method, also used by Najjar (1990), Najjar et al. (1992) and Murnane et al. (1999) for phosphate and Gnanadesikan (1999b) for silicate, utilizes the extensive spatial coverage of nutrient data to diagnose productivity. It implicitly accounts for effects of light and micronutrient limitation since where these occur, surface nutrient concentrations will be high. In contrast to much of the previous work using restoring, in which the nutrients were restored towards the annual average and the model was forced by annual averages of surface fluxes, in our work the surface nutrients were restored toward the seasonally varying nutrient fields from Louanchi and Najjar (2000, henceforth LN2000) and the circulation is also seasonal. The total production Jprod is time-dependent:

$$\mathrm{Jprod}(x,y,z,t) = (\mathrm{PO_4}(x,y,z,t) - \mathrm{PO_4^{obs}}(x,y,z,t))/T \quad z < 75\ \mathrm{m}\ \ \mathrm{PO_4} > \mathrm{PO_4^{obs}}, \tag{4}$$

where $T = 30$ days, $\mathrm{PO_4^{obs}}$ is the observed phosphate concentration, and $\mathrm{PO_4}$ is the simulated phosphate concentration.

The OCMIP 2 model makes an implicit assumption that all the nutrient taken up by phytoplankton is rapidly returned to the system. The organic matter produced by the restoring is instantly divided into two pools. One-third of the production is converted to particulate organic carbon, which is exported vertically and remineralized within the water column following the form proposed by Martin et al. (1987). If F_C is the vertical flux of material, then

$$F_C = F_C(z = z_c) * (z/z_c)^{\beta} \tag{5}$$

where z_c is the compensation depth, and β sets how quickly the flux decreases with depth. For the OCMIP 2 simulations, z_c was set to 75 m and β to -0.9, following Yamanaka and Tajika (1996).

It should be emphasized that the new production predicted by the model is sensitive to the shape of the remineralization profile. Gnanadesikan (1999b) looked at the cycle of silicon in a number of general circulation models with different dissolution parameterizations and eddy parameterization. This work demonstrated that large changes in dissolution schemes could result

in a factor of two change in the biogenic silica production within a single circulation scheme. The change was of the same order of magnitude as the change associated with changing the eddy parameterization and hence the circulation scheme. The changes in dissolution parameterization were much more extreme (all remineralization occurring on the bottom vs. one-half occurring in the upper kilometer) than those which would fit the range of sediment trap data. In order that the results here would be comparable with other OCMIP-2 type circulation models, we have not changed the remineralization scheme.

The portion of the production not exported as particulate organic matter goes into dissolved organic matter (DOM), which is advected and diffused with the water in which it is contained. Over time, this dissolved organic matter is remineralized to phosphate. Remineralization is modelled by assuming a decay of DOM governed by first-order kinetics with a rate constant of $1/6$ month^{-1}. Away from upwelling centers, the decay of dissolved organic matter is a major source of phosphate. Within the model, new production is defined as the net uptake of phosphate at a given point (the difference between the total production defined by (4) and the supply of phosphate due to remineralization of DOM above the compensation depth). New production is converted to carbon units using a Redfield ratio between carbon and phosphate of 117 (Anderson and Sarmiento, 1995).

It should be pointed out that restoring in the OCMIP 2 models occurs only within the top 75 m. This means that the model will miss production occurring at depths below 75 m, for example in the deep chlorophyll maximum. Secondly, the horizon for export is shallower than that usually used for export fluxes (generally 100 m or deeper). Insofar as the new and export production are often assumed to be equivalent, this mismatch will limit the comparability of the results here with estimates of export production. However, it should be noted that in the work of Laws et al. (2000), the majority of the cases considered (and all of those with high levels of productivity) involve net production at depths shallower than 75 m. Thus, while the estimate of new production made here may underestimate the true new production in regions such as the subtropical gyres, it is consistent with the estimates made in highly productive regions where the depth of the euphotic zone is shallow.

3.3. Estimating new production from dissolved nutrient variability

Najjar and Keeling (2000) and LN2000 recently used climatologies of dissolved oxygen, nitrate and phosphate to estimate new production. Starting with the data set of Conkright et al. (1994) they applied extensive quality control procedures to produce a data set that is relatively smooth in space and continuous in time. From the seasonal drawdown in phosphate and nitrate and the seasonal outgassing of oxygen from the mixed layer they produce an estimate of the new production. This method has the advantage that there is a much larger data set of surface nutrient and oxygen measurements than of primary productivity measurements, and also that the interpretation of such measurements is relatively straightforward.

However, as is recognized by the authors of both papers, there are significant weaknesses in such an approach. If nutrients are being supplied to the surface while new production is occurring, using the change in nutrients over the growing season will underestimate the magnitude of new production. Therefore, it will tend to underestimate new production in regions where there is strong upwelling or entrainment of nutrients from below. Chavez and Toggweiler (1995) estimate

upwelling to be a significant contributor to the global new production, accounting for 4.8 GtC yr^{-1} (essentially equivalent to the new production estimated by LN2000 from nutrient cycling). Our results support this conclusion. Gas exchange can also be a confounding factor for utilizing oxygen as a measure of new production. Although Najjar and Keeling (2000) do correct for gas exchange, there are significant uncertainties about what the correct piston velocity should be. For simplicity, we only consider the seasonal cycle of phosphate in this paper.

Our numerical model estimates are not independent of the LN2000 results, since their data set is used to force our model. As a result, in regions where there is significant upwelling and entrainment of nutrient-rich deep water, the seasonal variations of nutrient in the model will be similar to that in the LN2000 data set while the total new production will exceed that of LN2000. In such regions, the model-data comparison will yield primarily information about how much the variation in seasonal nutrients underestimates the true value of new production. However, as will be seen in Section 6.3, there are regions of the ocean where the models do not supply sufficient nutrients to the surface layer to maintain the phosphate concentrations seen in the LN2000 climatology. In such regions, the new production associated with seasonal nutrient variability provides an additional diagnostic of systematic weaknesses and biases in the models.

3.4. Estimating new production from satellite color

In order to estimate new production from ocean color, it is necessary to have both a method of estimating primary production and a robust relationship between primary and new production. In this paper, we use two estimates of primary production made using the method of Behrenfeld and Falkowski (1997a) (1997a, henceforth BF97a). Their method uses incident light and satellite-observed chlorophyll to produce an estimate of the net carbon fixed by biota. The total productivity PP_{eu} in mg C m^{-2} day^{-1} is given by

$$PP_{eu} = 0.66125 P^B_{opt} \frac{E_0}{E_0 + 4.1} C_{SAT} \times Z_{eu} \times D_{IRR} \tag{6}$$

where E_0 is the photosynthetically active irradiance in Einstein day^{-1}, C_{SAT} is the satellite-observed chlorophyll in mg Chl m^{-3}, Z_{eu} is the depth of the euphotic zone in m (defined as the 1% light level, and itself a function of the chlorophyll concentration), and D_{IRR} is the daily photoperiod in h day^{-1}. P^B_{opt} is a temperature-dependent "optimal" photosynthesis rate in mg C (mg Chl)$^{-1}$ h^{-1}. Chlorophyll is taken from the Coastal Zone Color Scanner (CZCS) data set of Feldman et al. (1989).

As noted by Behrenfeld and Falkowski (1997b), the major difference between primary production algorithms lies in the parameterization of P^B_{opt}. In this paper we use two parameterizations. The first is an eighth-order polynomial fit by BF97a to a large data set of primary production profiles (Fig. 3a). This curve is low at low temperatures, rises to a maximum at around 20°C, and drops off as the temperature increases yet further. The decrease at higher temperatures may implicitly parameterize the effects of iron limitation. A second parameterization is that of Eppley (1972, henceforth E72) in which $P^B_{opt} = 4.6 \times 1.065^{0.03(T-20)}$. The increase in P^B_{opt} accounts for the fact that the chemical reactions involved in photosynthesis act more quickly as temperature increases. BF97a show that the distribution of primary production predicted using this curve is essentially equivalent to the more complicated model of Antoine and Morel (1996).

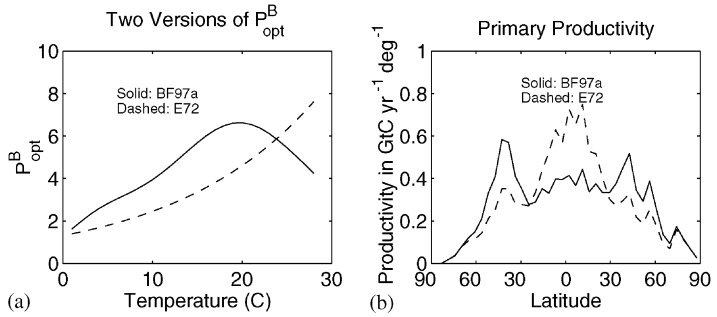

Fig. 3. P^B_{opt} and the spatial structure of satellite productivity. (a) Solid lines show P^B_{opt} from the data of Behrenfeld and Falkowski (1997a, BF97a), dashed lines show an exponential curve as in Eppley (1972, E72) with a carbon to chlorophyll ratio of 100. (b) Primary production calculated from the two curves using the CZCS satellite data.

As illustrated in Fig. 3b, these two parameterizations yield quite different regional estimates of primary productivity. Although the two curves both produce a global estimate of primary productivity of around 50 GtC yr^{-1}, the exponential P^B_{opt} yields a much larger primary production than the polynomial in tropical regions, and a lower primary production in the high northern latitudes. In the remainder of this paper, we will denote satellite productivity estimates made using the eighth-order polynomial as BF97a and that using the exponential formulation as E72.

A relationship between primary and new production, backed with a theoretical justification, was recently proposed by Laws et al. (2000). They constructed a multi-box model of an upper ocean food web, and chose system parameters that maximized the stability of the ecosystem, given varying ambient temperatures and rates of nutrient supply. Since the model does not include export of dissolved organic matter, the export and new production are equivalent, and Laws et al. (2000) refer to the ratio between the export and primary production as an ef-ratio. Although in the Laws et al. (2000) framework the e-ratio essentially controls the f-ratio, this would not necessarily be the case in the real ocean. Given that the data used to validate the model are all f-ratio data, it is at least possible that there could be systematic differences between the estimated f-ratio and the true f-ratio.

The Laws et al. model produces an f-ratio that is a function of productivity and temperature (Fig. 4a). When the productivity is very low, most production is recycled through the microbial loop, with only a little escaping to flagellates, ciliates, and filter feeders that export relatively high amounts of organic matter. The resulting ef-ratio is quite low (around 0.12). As productivity increases, more and more of the production goes through a pathway involving large phytoplankton and large grazers. The ef-ratio associated with this pathway is itself a function of temperature. As the temperature increases, grazers metabolize more and more of the ingested carbon and excrete a lower and lower fraction as exportable material. As a result, the actual f-ratio is a function of both temperature and productivity. Fig. 4b shows the zonal average ef-ratio derived from the zonally integrated primary production from the two satellite-based estimates and the zonally integrated new production derived from Laws et al. (2000). The curves are in close agreement throughout the world ocean. Essentially they both show low f-ratios (around 0.15)

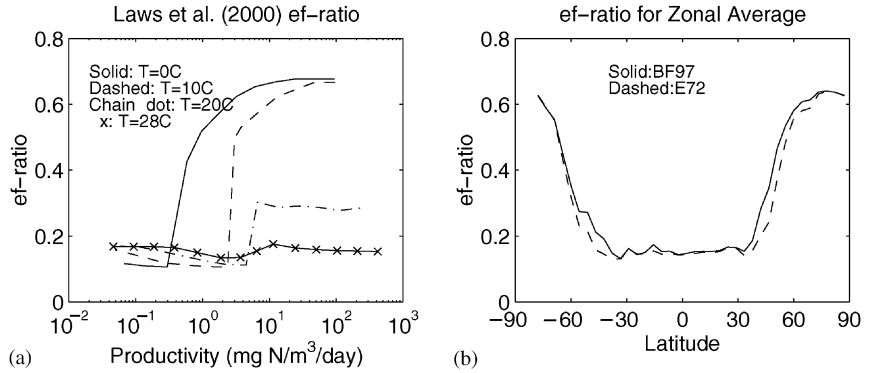

Fig. 4. New production vs. total production and temperature from the paper of Laws et al. (2000). (a) ef-ratio at high and low temperatures as a function of $\log_{10}$ total productivity. (b) ef-ratio for zonally integrated export and primary production using CZCS chlorophyll and BF97a and E72 P^B_{opt} and the Laws et al. (2000) formulation for ef-ratio.

equatorwards of 30° latitude, high export ratio (0.6–0.7) poleward of 60° latitude, with an essentially linear transition between these values in the zone of westerly winds. By applying these ef-ratios to the satellite-derived primary production, it is possible to come up with two consistent estimates of new production. The two satellite-derived estimates of new production will be denoted by BF97a + Laws for the estimate that uses primary production from Eq. (6) with the eighth-order curve of BF97a and the Laws et al. (2000) ef-ratio, and E72 + Laws for the estimate that uses an exponential P^B_{opt}.

4. Model results

4.1. Physical circulation

A major goal of circulation modelling is to produce a reasonable representation of the spatial variations in density within the global ocean. In a global average sense, the general circulation models are able to do a remarkably good job at simulating the depth of the pycnocline (as defined in Eq. (1)). Fig. 5 compares the predicted pycnocline depth from the six models with that found in the Levitus 1994 data set (Levitus and Boyer, 1994). The top panel shows three models (KVLOW + AILOW, KVHIGH + AIHIGH KVHISOUTH + AILOW) which do a good job at reproducing the observed pycnocline depth within the tropical oceans. All three models also track each other in the northern subtropics, with differences between the models primarily appearing in the Southern Ocean. This panel shows quite clearly that models with significantly different physics can nonetheless produce large-scale density structures that are very similar. The bottom panel shows the three other models. KVLOW + AIHIGH systematically underpredicts pycnocline depth, as would be expected from the theoretical scaling. KVHIGH + AILOW systematically overpredicts the pycnocline depth, also in accordance with the predictions of the theoretical scaling. KVHIMIX + AILOW is very similar to the models in the top panel. These simulations demonstrate that the zonally averaged pycnocline depth is sensitive to changes in the lateral and

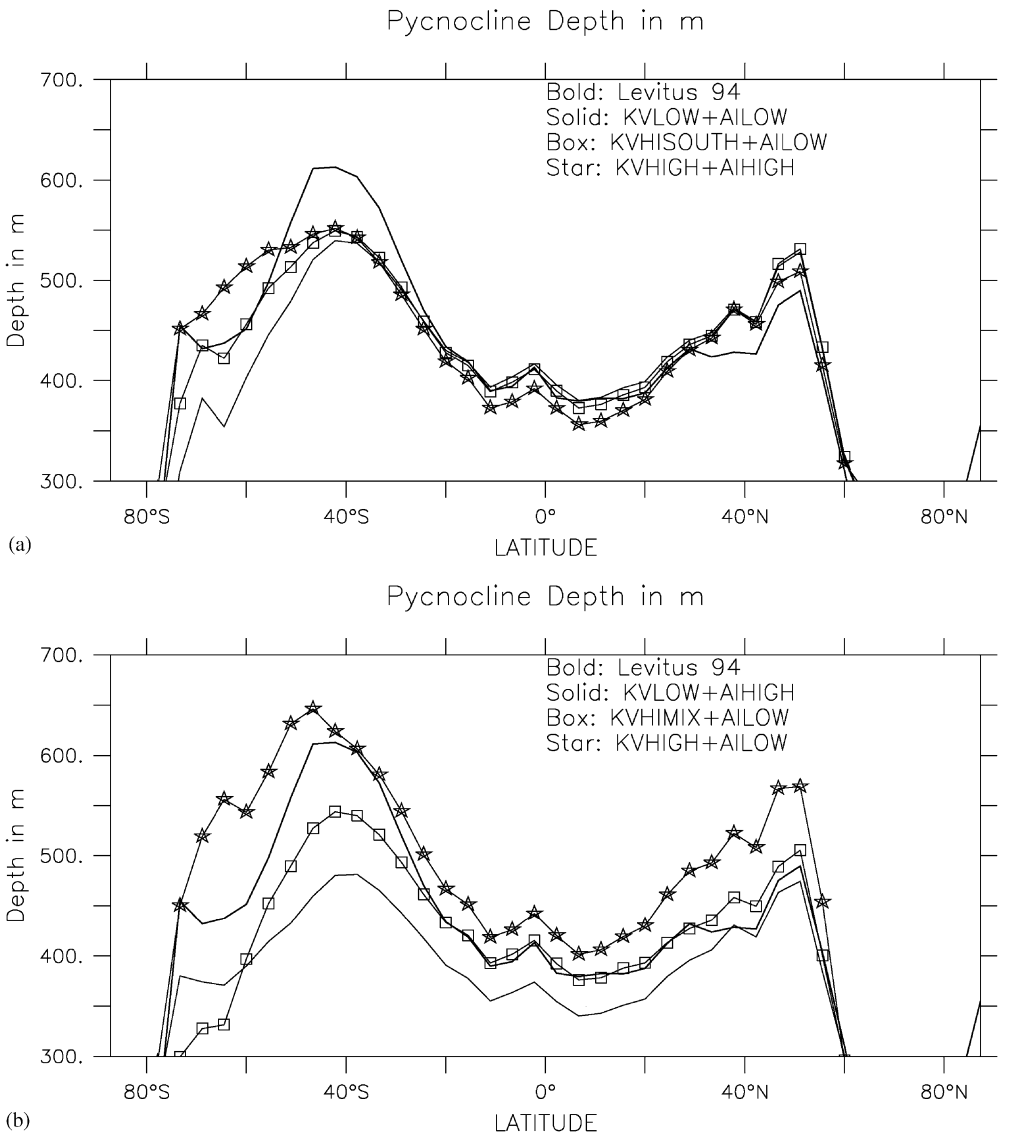

Fig. 5. Zonally averaged pycnocline depth. (a) Three cases which match data (bold) well in tropical latitudes. KVLOW + AILOW is shown by the solid line with no symbols, KVHISOUTH + AILOW by the solid line with boxes and KVHIGH + AIHIGH by the solid line with stars. (b) Three other cases. KVLOW + AIHIGH is shown by the solid line with no symbols, KVHIMIX + AILOW by the solid line with boxes, and KVHIGH + AILOW by the solid line with stars. Note that KVHIGH + AILOW is systematically high, while KVLOW + AIHIGH is systematically low.

vertical mixing, but relatively insensitive to large changes of the mixing coefficient within the top 50 m.

The zonally averaged temperature fields generally reinforce the picture emerging from Fig. 5. Fig. 6 shows the zonally averaged temperature errors (model temperatures vs. the Levitus 1994 data set) associated with the baseline suite of four runs. KVLOW + AILOW and

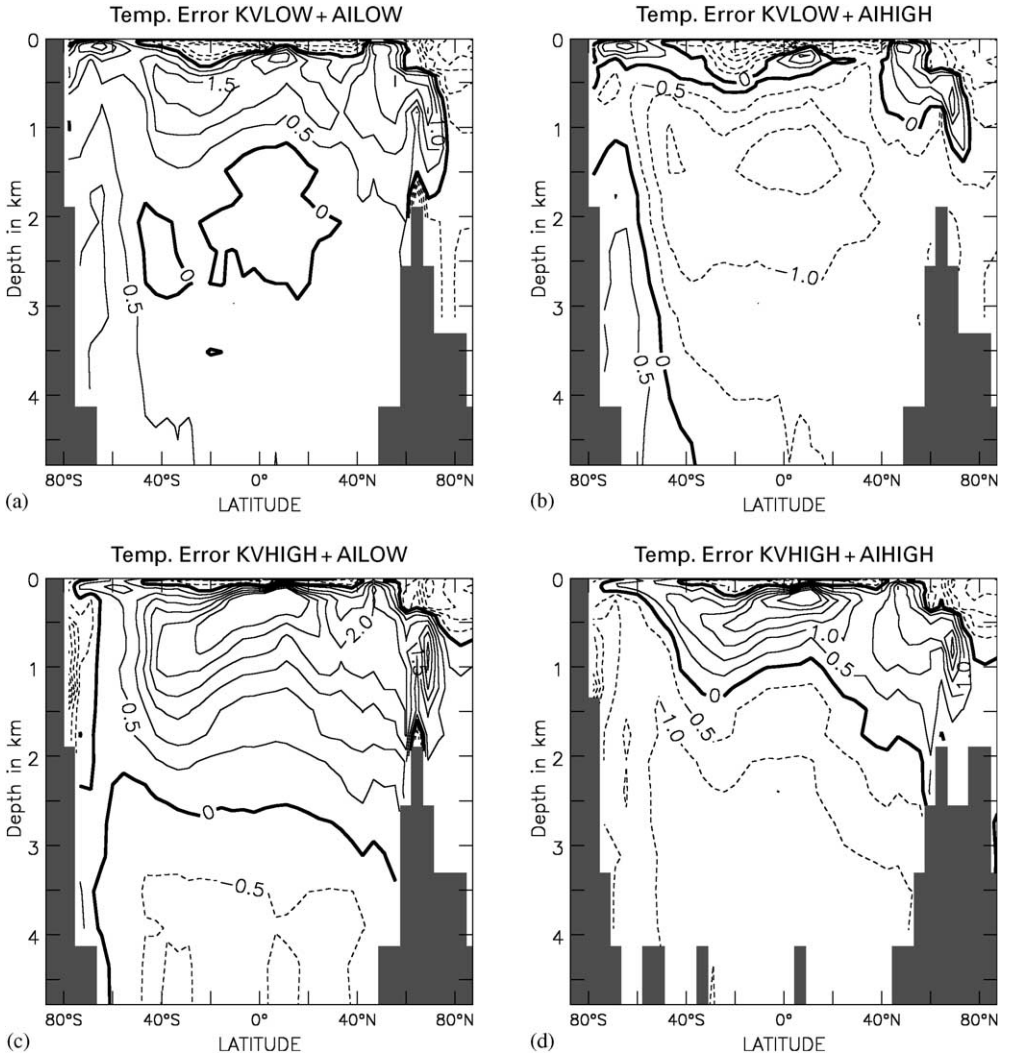

Fig. 6. Zonally averaged temperature error (model-Levitus climatology) in degrees for the baseline suite of four models. (a) KVLOW + AILOW. (b) KVLOW + AIHIGH. Temperatures in this run are too cold throughout the water column. (c) KVHIGH + AILOW. The thermocline is far too warm in this run. (d) KVHIGH + AIHIGH. Thermocline temperatures are quite similar to KVLOW + AILOW, although deep temperatures are lower.

KVHIGH + AIHIGH have very similar zonally averaged temperature fields in the top km of the water column. The horizontally averaged temperatures in these two models are within 1° of the Levitus data set throughout the upper water column. By contrast, temperatures in the KVHIGH + AILOW simulation are systematically too high in the upper pycnocline, while KVLOW + AIHIGH has a wind-driven pycnocline that is too cold, waters around 300 m that are slightly too warm (though closer to observations than in any of the other runs), and an abyss that is too cold. The errors in salinity (not shown) tend to mirror those in temperature, but have a partially compensating effect with respect to density (warm waters tend to be too salty, cold waters too fresh).

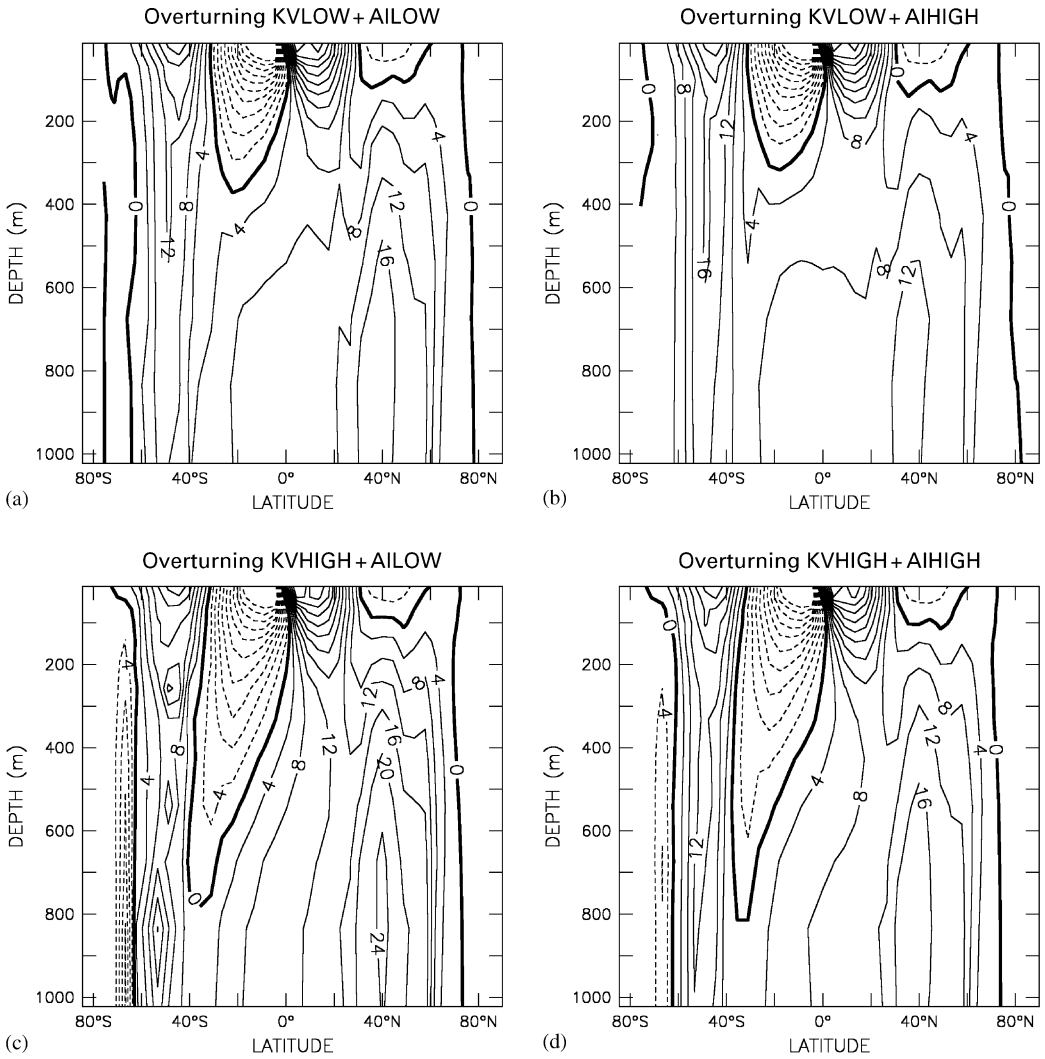

Fig. 7. Overturning streamfunction in Sv in the baseline suite of four models. Positive values are clockwise. (a) KVLOW + AILOW. (b) KVLOW + AIHIGH. (c) KVHIGH + AILOW. (d) KVHIGH + AIHIGH.

Despite the similarities in pycnocline structure, there are significant differences in the large-scale circulation between the different simulations. The overturning streamfunctions associated with the four baseline models are shown in Fig. 7. In model KVLOW + AILOW a small fraction of the water that upwells through the tropical pycnocline comes from below the pycnocline depth of around 600 m. Between 30S and 30N, there is only 8 Sv of upwelling across 600 m. This value is in rough agreement with the value predicted from Eq. (3). The majority of this upwelling ends up reaching the surface in the northern oceans rather than passing through the tropical pycnocline. Only 2.2 Sv upwells across 300 m depth in the low latitudes. By contrast in the two cases with KVHIGH, there is a great deal of upwelling across 600 m (16.5–20.5 Sv), of which

almost 80% upwells across 300 m. The difference in upwelling between KVLOW + AILOW and KVHIGH + AIHIGH is close to that which would be expected from the theoretical scaling of Gnanadesikan (1999a). The increase in pycnocline depth between KVLOW + AILOW and KVHIGH + AILOW is also correlated with an increase in northern hemisphere overturning, as expected from the theory. In the KVHIGH simulations the northern overturning is more directly connected to the tropical surface. Note that it is the pathway involved in returning the northern hemisphere overturning that changes between KVLOW + AILOW and KVHIGH + AIHIGH. The volume transport of the northern hemisphere sinking is essentially the same in both cases.

The dependence of the overturning on lateral diffusion is less clearly explicable. Increasing the lateral diffusion reduces both the northern hemisphere sinking flux and the magnitude of the deep upwelling flux. Although the deep upwelling decreases only modestly (from 8 to 4 Sv across 600 m in the KVLOW cases and from 20.5 to 16.5 Sv for the KVHIGH cases), this change is opposite to that found by Gnanadesikan (1999a), where a slight increase in low-latitude upwelling was found as A_I was increased. The reasons for the difference are unclear. It is possible that the difference arises from differences in the surface boundary conditions. Gnanadesikan (1999a) used fixed surface restoring boundary conditions, which resulted in a relatively fixed lateral density gradient, whereas the present study uses a combination of flux and restoring boundary conditions.

It is important to realize that not all changes in the mixing coefficient have an impact on the pathways of upwelling or low-latitude pycnocline. As shown in Fig. 8, there is little difference between the KVHISOUTH + AILOW and KVLOW + AILOW runs in the low-latitude thermocline. Both the temperatures and upwelling are essentially unchanged in these latitudes. Temperatures within the Southern Ocean and in the deep waters that are ventilated from the south do show a cooling, and the deep overturning of Antarctic Bottom Water increases slightly. This result highlights the fact that it is the value of K_v within the *low-latitude* pycnocline rather

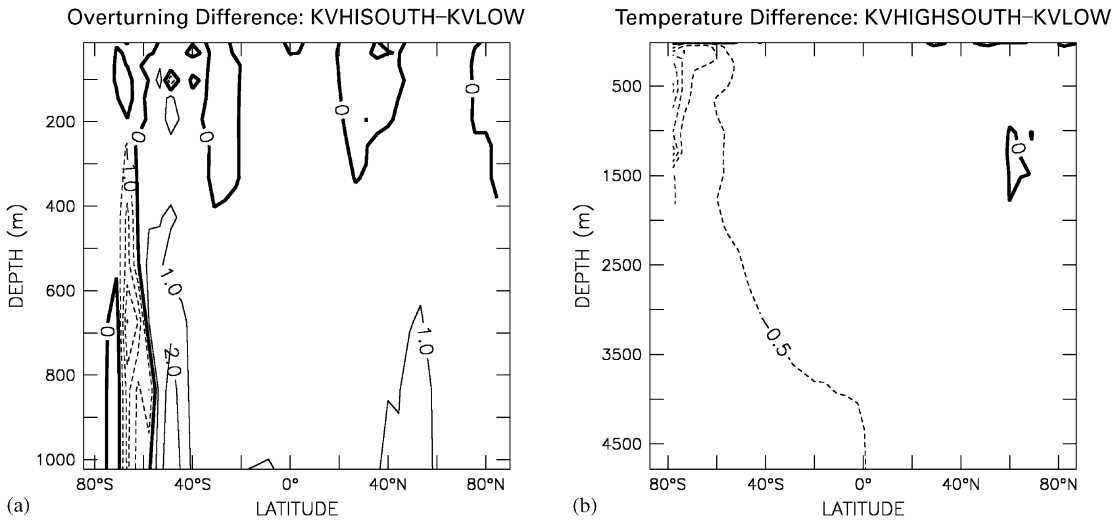

Fig. 8. Differences in temperature and overturning streamfunction between KVHISOUTH + AILOW and KVLOW + AILOW (KVHISOUTH-KVLOW). (a) Overturning streamfunction in Sv. Note that all the change is below the low-latitude thermocline. (b) Temperature. Changes are primarily in waters ventilated from the deep Southern Ocean.

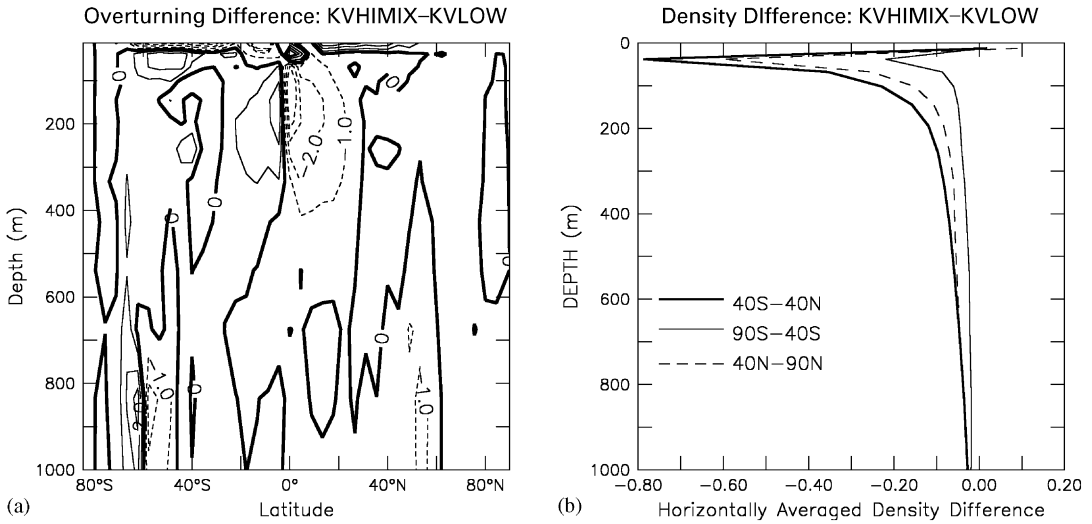

Fig. 9. Differences in overturning streamfunction and density between KVHIMIX + AILOW and KVLOW + AILOW (KVHIMIX-KVLOW). (a) Overturning streamfunction in Sv. The equatorial upwelling circulation weakens slightly in this run. (b) σ_θ in kg m^{-3}. Differences are quite large, but are primarily trapped to the surface waters.

than some global-average value which determines how the North Atlantic Deep Water is transformed back to light surface waters.

Increasing K_v within the surface layer primarily affects the density structure in low latitudes. As shown in Fig. 9b, relative to KVLOW + AILOW, surface densities do not change substantially in model KVHIMIX + AILOW, but waters immediately below the surface layer become substantially lighter. In low latitudes, this is most likely because light surface water is more effectively stirred down. At high latitudes, the effect can be understood in the context of a seasonal cycle of surface density. In a model with very low vertical diffusion, during periods when the surface water is becoming lighter convection is shut off and the light water is trapped near the surface. When the surface water becomes denser in such a model, however, convection spreads this signal into the deep. Thus the waters in the top few hundred meters tend to reflect the wintertime densities within the surface layer, but not the summertime densities. Increasing the mixed layer diffusivity tends to counteract the trapping of the light surface waters, and so tends to decrease the density of the waters immediately below the surface layer. At depth, however, there is little change in the temperature or density. The reduction in subsurface density is most pronounced in the low latitudes but is also significant in northern latitudes.

In addition to affecting the pathways of advection, changes in K_v and A_I also affect the distribution and intensity of convection. The changes are illustrated in Fig. 10, which shows the zonally and temporally averaged convective index. The convective index is set to 1.0 within the model when convection affects a grid cell, and is set to zero otherwise. A value of 1.0 means that all the points at a particular level and latitude are convecting all the time. Convection in level-coordinate models can occur both as a result of surface forcing and as a result of numerical discretization of advective processes. An example of convection driven by numerical processes is found when cold water flowing off a shelf cannot follow the bottom in a level-coordinate model.

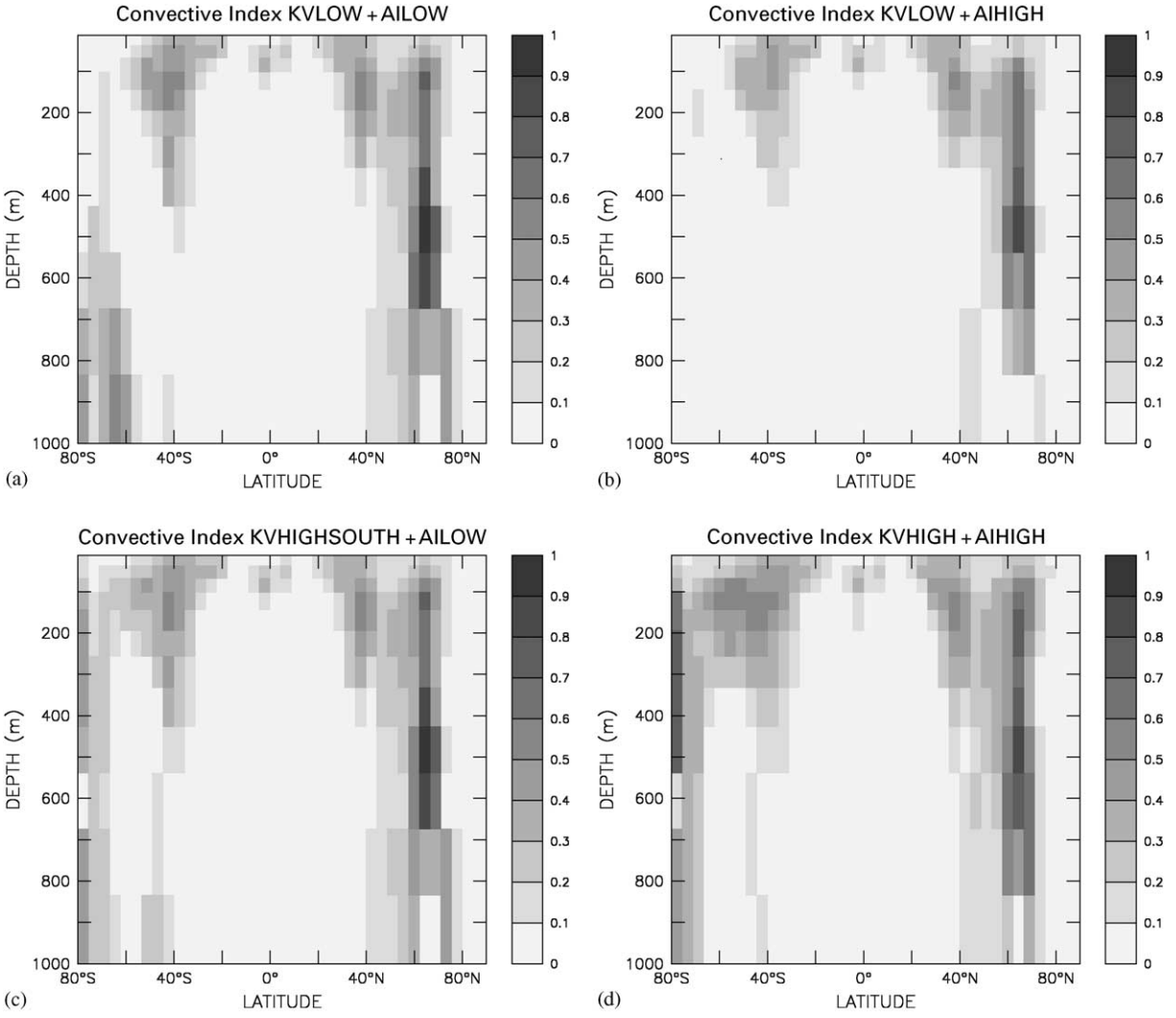

Fig. 10. Zonally averaged convective index for four of the six models. Convective index is set to 1 whenever convection is turned on, so that a value of 0.5 can either mean that half of all points at a particular depth and latitude are convecting all the time, that all of the points at particular depth and latitude convect half the time, or something in between these two extremes. (a) KVLOW + AILOW. (b) KVLOW + AIHIGH. Note the suppression of convection relative to (a). (c) KVHISOUTH + AILOW note the increase of convection near the Antarctic continent relative to (a). (d) KVHIGH + AIHIGH. Note the increase in convection relative to the other three figures.

As a result, it flows horizontally into the interior, where it is denser than the water beneath it and mixes convectively (Winton et al., 1998). Convection also may occur as the result of inaccuracies in the discretization of tracer transport (Griffies et al., 2000). These facts should be considered in interpreting the distribution of convection in Fig. 10, in which not all the convection seen is driven by surface forcing.

Increasing the isopycnal diffusion coefficient A_I reduces convection. This can be seen by comparing Fig. 10a and b, showing runs KVLOW + AILOW and KVLOW + AIHIGH, respectively. The former simulation has significant amounts of convection around the margin of Antarctica, which vanishes when A_I is increased. The extent of the other convective zones also contracts slightly and the magnitude of the maximum convective index is slightly reduced (though this last effect is not easily visible in the figure). The reason for this change is that the increased diffusion coefficient results in a more efficient diffusion of layer thickness, flattening isopycnals and stabilizing the water column.

By constrast, increasing the vertical diffusion coefficient K_v, either within the Southern Ocean (compare Fig. 10a and c) or globally (compare Fig. 10b and d) increases the extent and intensity of convection. For both KVHISOUTH + AILOW and KVHIGH + AIHIGH, the largest changes are seen in the Southern Ocean, polewards of 60S. Interestingly, the largest increases in convection are associated with the fourfold increase of K_v throughout the entire ocean, rather than with an even larger increase of K_v in just the Southern Ocean.

The differences in convection become very evident in the distribution of transient tracers such as CFC-11 (Fig. 11) of passive tracers. In addition to the carbon cycle simulations, experiments also were made in which the atmospheric concentration of CFC-11 was prescribed according to reconstructed historical concentrations (Walker et al., 2000). CFC-11 was then allowed to invade the ocean following the OCMIP-2 protocols (Dutay et al., 2001). The zonally averaged concentration of CFC-11 in the year 1995 is shown in Fig. 11a. High concentrations are seen in the intermediate waters and in the formation region for North Atlantic Deep Water. As shown in

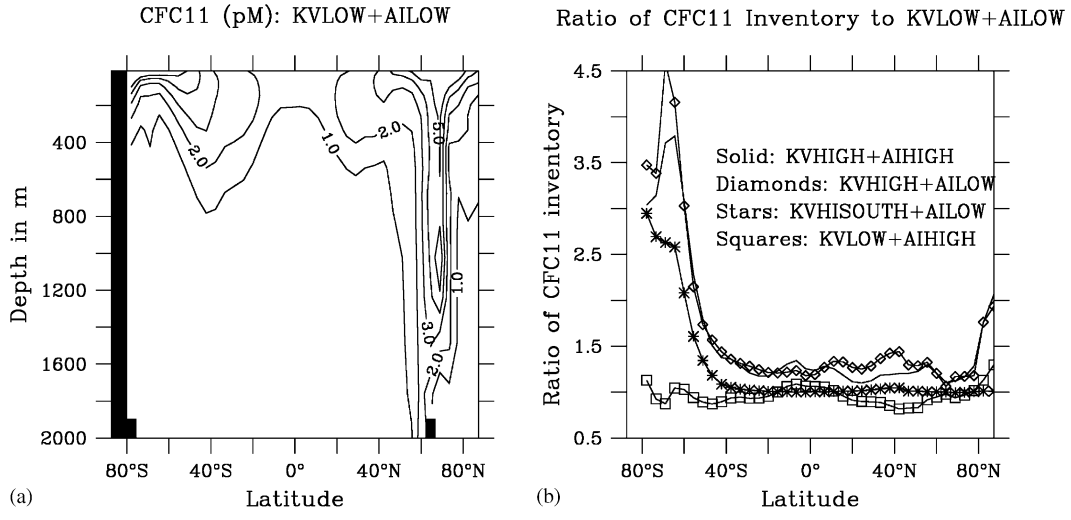

Fig. 11. CFC uptake in the different models. (a) Zonally averaged CFC-11 concentration in pM/l for model run KVLOW + AILOW. (b) Ratio of CFC-11 inventory in other models to that in KVLOW + AILOW. Solid: KVHIGH + AIHIGH. Note that this run has a large increase in the far southern latitudes, but a relatively modest increase in low latitudes. Diamonds: KVHIGH + AILOW. This has an even larger increase in high Southern latitudes, but is quite similar to KVHIGH + AIHIGH in low latitudes. Stars: KVHISOUTH + AILOW. This model has a very similar inventory (ratio is close to 1) north of 40S, but shows the effects of increased convection to the south of 40S. Squares: KVLOW + AIHIGH. This model has very similar inventories of CFC11 at all latitudes.

Fig. 11b the different models have significantly different inventories of CFC-11. The differences are largest in very high southern latitudes (a factor of 3–4) but are relatively small (25% or so) away from the Antarctic and Arctic Oceans. Dutay et al. (2001) show that the KVLOW + AILOW model greatly underpredicts the uptake of CFC-11 within the Southern Ocean. As will be shown in the following section, new production shows a very different sensitivity to mixing, with the subtropical gyres and low latitudes also showing a strong sensitivity to the rate of diapycnal mixing.

4.2. New production in the circulation models: general results

One of the reasons we chose to examine new production as a tracer of circulation was the hope that it would be much more sensitive to vertical exchange than traditional tracers of ventilation such as bomb radiocarbon or CFCs. That this is plausible can be seen by considering the following thought experiment. Suppose a parcel of water is brought to the surface, stripped of nutrients, transported to depth where nutrients are added, and brought back to the surface again without exchanging fluid with its surroundings. The new production associated with this process is proportional to the rate at which this cycle occurs. By contrast, if we consider a parcel of water that comes to the surface, takes up CFCs, is transported to depth, and then comes to the surface again, uptake of CFC will only be proportional to the rate of exchange if the time taken to complete the cycle is longer than the time over which the atmospheric concentration of CFC changes substantially. A parcel that returns to the surface after 2 years will not take up half as much CFC as one which returns to the surface after 1 year. In fact, the uptake of CFC will be more or less the same, while the new production will be half as large.

As can be seen from Fig. 12 and Table 1 the new production has a very different response than the CFC inventory to changes in mixing parameters. This is especially true in the low latitudes. For example, while near-equatorial inventories of CFC-11 varied only by about 30%, new production varies by more than a factor of two between the models (Fig. 12b). Even larger increases in new production are seen within the subtropical gyres, where KVLOW + AILOW predicts very low values.

The largest sensitivity is seen for K_v. The models with KVHIGH have roughly twice the level of new production as the models with KVLOW. This effect is seen at all latitudes. The two models with KVHIGH predict a total new production of 19.2 (AIHIGH) and 22.4 GtC yr^{-1} (AILOW) (Table 1, column 1) while the two models with KVLOW have global new production estimates of 9.0 (AIHIGH) and 10.5 GtC yr^{-1} (AILOW).

It is interesting to compare the various models with AILOW (KVLOW, KVHIGH, KVHISOUTH and KVHIMIX). Increasing the vertical diffusion coefficient away from the mixed layer increases the production. When K_v is increased uniformly (KVHIGH) the effect is seen in all regions. By contrast, when K_v is only increased within the Southern Ocean (KVHISOUTH), the bulk of the increase in production occurs within the Southern Ocean, with little to no change in low latitudes (see Table 2). Somewhat surprisingly, increasing the mixing within the mixed layer alone (KVHIMIX) has the opposite effect, reducing production slightly in all regions, but most especially in the highly productive ones (see Table 2). This is consistent with the lightening of waters immediately below the surface layer seen in Fig. 9. Lightening these waters decreases the rate at which they exchange with the nutrient-rich abyss. In general, the

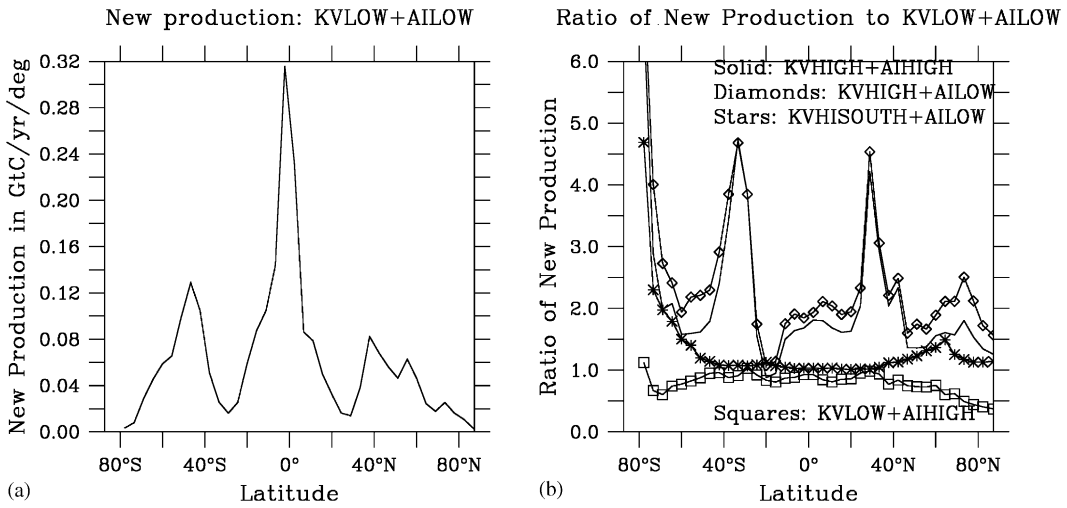

Fig. 12. New production (defined as net phosphate uptake) in the different models. (a) Zonally-integrated new production in GtC yr^{-1} deg^{-1} for model run KVLOW + AILOW. (b) Ratio of new production in other models to that in KVLOW + AILOW. Solid: KVHIGH + AIHIGH. Note the large increases throughout the model domain, a major contrast to the CFC inventory. Diamonds: KVHIGH + AILOW. This run is quite similar to KVHIGH + AIHIGH in low latitudes. Stars: KVHISOUTH + AILOW. This model has a very similar inventory (ratio is close to 1) north of 40S, but shows the effects of increased convection to the south of 40S. Squares: KVLOW + AIHIGH. This model has significantly lower new production.

Table 1
Annual new production by basin in units of GtC yr^{-1}[a]

	Global	Atlantic	Pacific	Indian	N.N. Atl.	N.N.Pac
KVLOW + AILOW	10.6	3.8	4.6	1.6	1.3	0.23
KVLOW + AIHIGH	9.0	2.8	4.3	1.5	0.8	0.21
KVHIGH + AILOW	22.4	6.9	9.4	4.7	2.5	0.30
KVHIGH + AIHIGH	19.2	5.6	8.6	3.8	1.9	0.33
KVHISOUTH + AILOW	12.1	4.9	4.8	1.8	1.6	0.24
KVHIMIX + AILOW	9.3	3.3	4.0	1.5	1.0	0.22
BF97a + Laws	12.3	5.5	4.8	1.5	3.3	1.5
E72 + Laws	10.2	4.3	3.8	1.8	2.3	0.8
LN2000 (PO_4)	5.3	1.3	2.6	1.1	0.3	0.6

[a] The Northern North Atlantic and Northern North Pacific are those parts of the basins to the north of 40N. The top six rows are for the six model runs described in the text, while the bottom three represent three separate observational estimates, BF97a and E72 using satellite color and LN2000 using the annual cycle of nutrients. Our estimates used LN2000's data mapped to our grid. Regional numbers do not necessarily add up to global numbers because of the exclusion of marginal seas.

effects of changing the mixing coefficient within the mixed layer alone (KVHIMIX) are relatively small. Increasing the mixed layer diffusivity reduces the new production by 10–20%, with the largest changes occurring in the North Atlantic. The fact that increasing K_v can result in a lower production illustrates that the effect of mixing on the global-scale vertical exchange is not simple.

Table 2
Same as Table 1, but broken down latitude band in units of GtC yr^{-1}

	90S–60S	60S–40S	40S–20S	20S–20N	20N–40N	40N–90N
KVLOW + AILOW	0.5	1.9	0.7	5.1	0.7	1.7
KVLOW + AIHIGH	0.4	1.7	0.6	4.5	0.6	1.2
KVHIGH + AILOW	1.3	4.5	2.0	9.3	1.9	3.3
KVHIGH + AIHIGH	1.0	3.5	1.9	8.2	1.8	2.7
KVHISOUTH + AILOW	1.0	2.3	0.7	5.3	0.8	2.0
KVHIMIX + AILOW	0.5	1.7	0.6	4.4	0.6	1.4
BF97a + Laws	0.8	1.5	1.1	2.5	1.1	5.1
E72 + Laws	0.7	0.7	0.7	3.8	0.9	3.3
LN2000 (PO_4)	0.6	1.6	0.9	1.0	0.3	1.0

The new production is substantially less sensitive to increases in A_I than to changes in K_v. Changes in A_I which produce an equivalent effect on the density structure as changes in K_v have a much smaller effect on the new production. Increasing A_I reduces the new production in the Subantarctic zone (60S–40S) for both KVLOW and KVHIGH, and reduces new production by 25–30% in the North Atlantic. This change is considerably smaller than the factor of 2 change associated with changing K_v.

It is instructive to examine why K_v has such a large effect on production. Fig. 13 shows the vertical flux of nutrient (normalized to carbon units) due to various processes integrated globally for five of the model runs (excluding KVHIMIX + AILOW, which is essentially identical to KVLOW + AILOW away from the topmost three boxes). The processes considered are: (1) vertical advection (excluding the eddy induced velocities of Gent and McWilliams, 1990), (2) convection, (3) vertical advection due to eddies, and (4) vertical diffusion (including the isopycnal component of vertical diffusion). Several features stand out in this figure. The first is that increasing the vertical diffusion coefficient increases the advective and convective as well as the diffusive supply of nutrient. On a global scale, the largest change in vertical phosphate flux between KVLOW + AILOW (solid dashed lines) and KVHIGH + AILOW (bold dashed lines) is seen in the convection, which increases from 2.4 to 8.5 GtC yr^{-1} across 85 m, a factor of 3.5 increase. The vertical diffusive flux of phosphate shows a somewhat less extreme response, doubling from 4 to 8 GtC yr^{-1}. The vertical advective flux of phosphate also rises from 4.8 to 6.5 GtC yr^{-1}, an increase of 35%. The total increase in the convective and advective fluxes together is twice that of the diffusive flux.

A second lesson of Fig. 13 is that changes in lateral diffusion have a relatively small, but still significant, effect on the fluxes. The largest effect is seen in the convective flux. The convective supply of nutrient across 85 m drops by 20–35% as A_I is doubled. The vertical diffusive flux of nutrient also decreases as A_I increases, dropping from 8.0 GtC yr^{-1} in KVHIGH + AILOW to 6.9 GtC yr^{-1} in KVHIGH + AIHIGH. The decrease in vertical diffusive flux as A_I increases is not intuitive, as it might be thought that a larger eddy diffusion coefficient would bring up more nutrients along sloping isopycnals. In fact, however, the increase in A_I tends to reduce the isopycnal slope, cancelling the effect of increasing the diffusion coefficient.

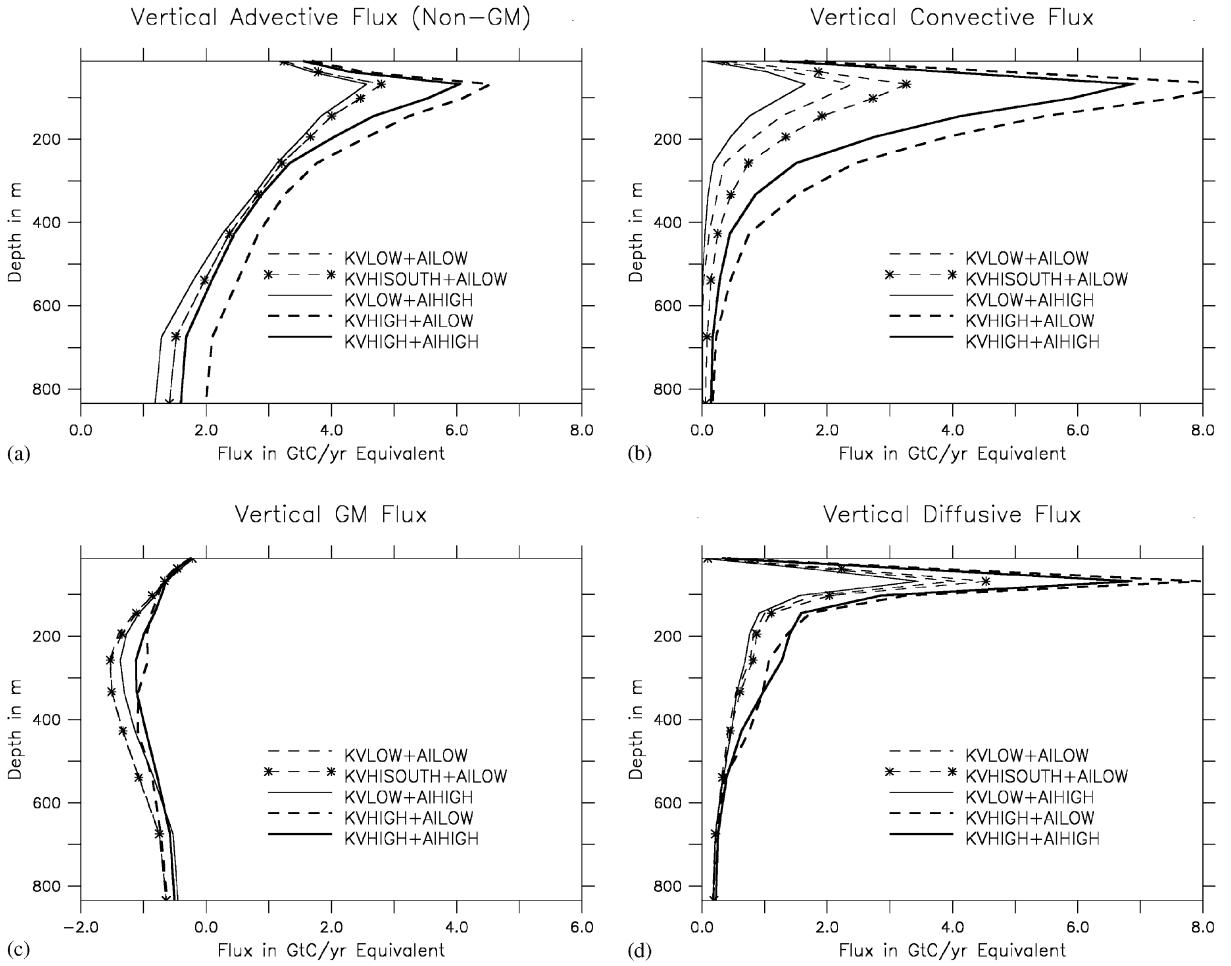

Fig. 13. Vertical flux of phosphate (converted to the equivalent flux of carbon in GtC yr^{-1}) carried by different physical processes, integrated over the entire ocean in different simulations. (a) Vertical advective flux excluding the component due to eddies (Gent and McWilliams, 1990). (b) Convection. (c) Vertical advective flux due to eddies. (d) Vertical diffusive flux.

A final lesson from Fig. 13 is that the relative importance of the three main pathways of nutrient supply changes with depth. At the surface, convection plays an important role. At depth, advection is far more important. At 1000 m, the vertical advective flux of phosphate shows the largest impact of the changes in diffusion, ranging from a minimum of 0.8 GtC yr^{-1} (KVLOW + AIHIGH) to a maximum of 1.6 GtC yr^{-1} (KVHIGH + AILOW).

The relative importance of the three main pathways of supply differs greatly by region. This is illustrated in Fig. 14a, which shows the difference in the vertical phosphate flux between KVHIGH + AIHIGH and KVLOW + AILOW at 85 m. In the equatorial zone (10N–10S), the largest differences are seen in the vertical advective flux. As would be expected from the overturning streamfunction, in the low latitudes increasing K_v increases the upwelling of nutrient-

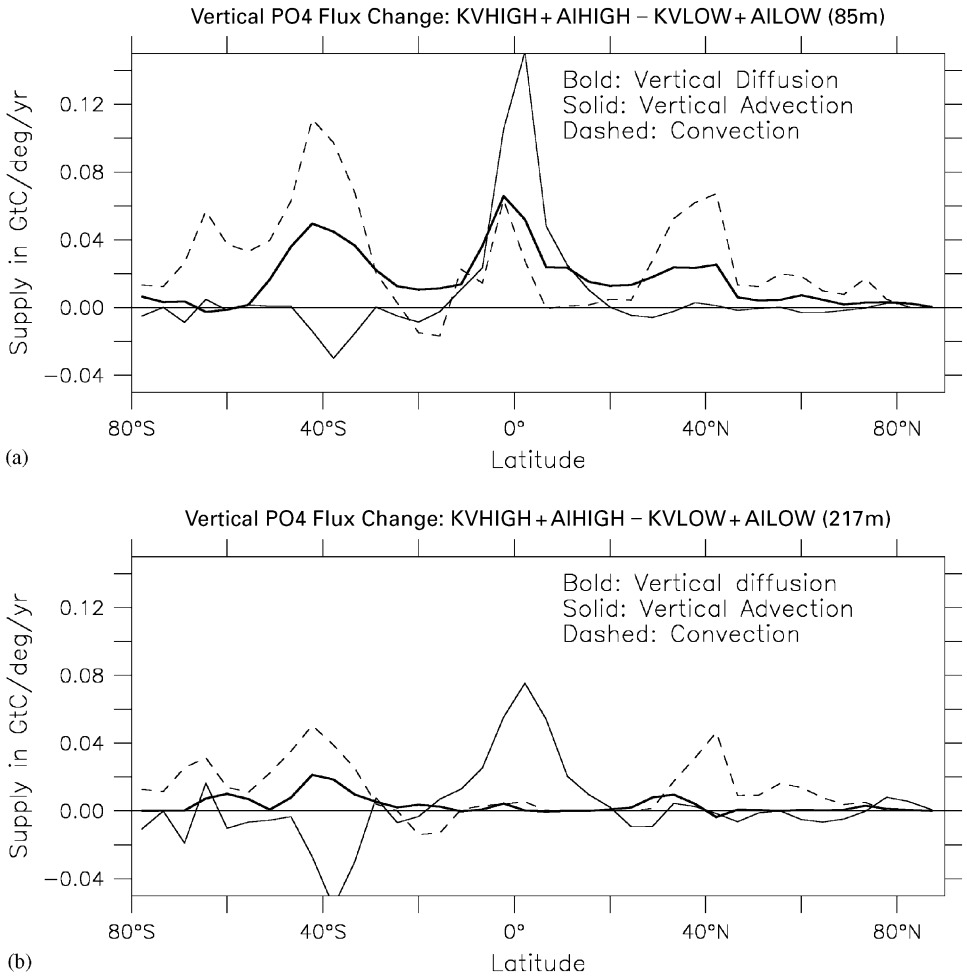

Fig. 14. Change in the vertical flux of phosphate in GtC yr^{-1} deg^{-1} equivalents between KVHIGH + AIHIGH and KVLOW + AILOW. Bold lines are the total vertical diffusive flux, solid lines the advective flux, and dashed lines the convective flux. (a) Flux into the euphotic zone (across a depth of 85 m, the bottom of the lowest box in which production occurs). (b) Flux across a depth of 217 m. Note that vertical diffusion now changes very little, while vertical advection is still important.

rich abyssal water through the tropical pycnocline. This increased advective flux can be seen at 217 m as well (Fig. 14b) though it is more spread out at this depth. By contrast, the vertical diffusive flux is very similar at a depth of 217 m. Apparently, the reduction in isopycnal slope associated with the higher lateral mixing as well as a readjustment of the phosphate field essentially compensates for the change in vertical mixing.

By contrast, in the latitude bands between about 10° and 30°, the most important change in the pathway of nutrient supply is associated with vertical diffusion. This is the region associated with the largest relative change in production between the high- and low-mixing cases in Fig. 12. It is dominated by the poleward advection of warm, nutrient-depleted surface waters, so that neither

advection nor convection is a major source of nutrients. Thus, this region is especially sensitive to changes in K_v.

Polewards of about 30°, changes in convection dominate the changes in the vertical flux of phosphate, though changes in vertical diffusion sometimes may be substantial as well. Such changes might be expected from the difference in the convective index between KVLOW + AILOW (Fig. 10a) and KVHIGH + AIHIGH (Fig. 10b). What is striking, however, is how dominant these changes are, particularly in the far Southern Ocean, poleward of 60S.

The changes in the pathways of phosphate supply illustrate that the relationships between different transport processes make it necessary to use circulation models to understand the true sensitivity of biogeochemical cycling to physical parameterizations of mixing. The vertical and lateral diffusion coefficients affect not only the diffusive flux of tracers, but the density structure of the ocean in subtle, regionally dependent ways. As such, they alter the convective and advective fluxes in ways which are not simple. The indirect effects of changing the diffusion coefficients may dwarf or mask their direct effect on the vertical diffusive flux.

5. Comparison between model and observationally based estimates

On a global scale the observationally based estimates of new production lie towards the lower end of the range of models (Tables 1 and 2). The globally integrated satellite estimates of new production (shown in the first column of Table 1) are 12.3 GtC yr^{-1} for BF97a + Laws and 10.2 GtC yr^{-1} for E72 + Laws. Of the four baseline models KVLOW + AILOW produces a global new production value (10.6 GtC yr^{-1}) that is most consistent with the two satellite-based estimates. The KVHIGH models by contrast, predict a value of new production that is substantially larger than the satellite-based estimates.

As noted above, the models can be used to estimate the size of the underestimate in the new production estimated from seasonal variations in dissolved nutrient. Fig. 15 shows the model new production as well as that inferred from the annual range of phosphate (dashed lines) in KVLOW + AILOW and KVHIGH + AIHIGH. In both models, inferring the production from annual range of surface properties significantly underestimates the total production. As expected, this underestimate is the largest in the zones where there is upwelling and relatively small in the subtropical gyres. The size of the underestimate depends on the model physics. For KVLOW + AILOW, the seasonal variability of phosphate yields a value of 5.7 GtC yr^{-1}. This estimate is 55% of the actual new production of 10.6 GtC yr^{-1} calculated by the model. When the vertical diffusion increases, the size of the underestimate implicit in using annual range of nutrients increases as well. For KVHIGH + AIHIGH, the annual range in phosphate yields a value of 7.3 GtC yr^{-1}, only about 40% of the total new production of 19.2 GtC yr^{-1}.

The models with lower values of mixing also agree reasonably well with satellite-based estimates when it comes to interbasin partitioning of the new production. The satellites show approximately equal levels of new production in the Atlantic and Pacific Oceans, with 1/2–1/3 the value in the Indian Ocean. Although the KVHIGH models change the partitioning somewhat, so that the Indian Ocean is a slightly larger fraction of the total production and the Atlantic is a slightly lower fraction of the total production (closer to 30% than 40%), the interbasin partitioning still mirrors

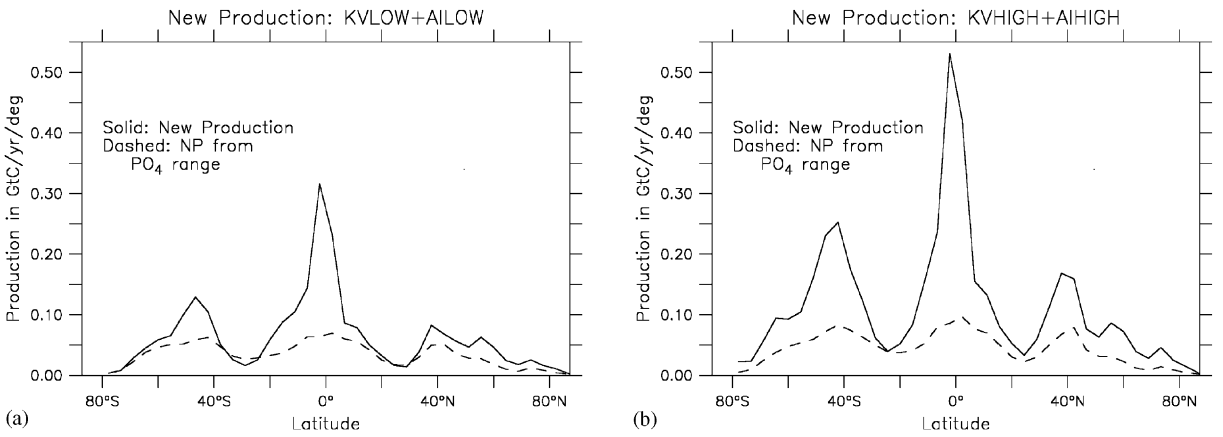

Fig. 15. Model-based estimate of the underestimate in new production inherent in the seasonal nutrient range method of LN2000 Solid lines are the model productivity, dashed lines the productivity estimated from annual phosphate range within the model. (a) KVLOW + AILOW. (b) KVHIGH + AIHIGH.

that estimated from the satellites. The fact that the average rate of production in the Atlantic is much higher than in the Pacific is due in large part to very high levels of new production in the Northern North Atlantic. This region by itself accounts for 10–15% of the new production in the models and around 25% in the satellite-based estimates.

Significant disagreements emerge, however, when zonal averages are taken (Fig. 16, Table 2). The models all show a pattern of high new production regions with upwelling and/or mode water formation and lower new production in downwelling zones. The satellite-based estimates do not always reflect this pattern. The E72 + Laws estimate of new production, for example, does not show any differences between the southern substropical gyres and the Southern Ocean. The lower chlorophyll values in the gyres are apparently balanced by a higher P^B_{opt} associated with higher temperatures. By contrast, the BF97a + Laws estimate distributes production relatively evenly among all latitudes within the trade wind band. Both the satellite-based estimates have a significant fraction of the production in latitudes north of 40N (25% for E72 + Laws and 37% for BF97a + Laws) while the GCMs predict only 12–15%.

In the face of these large regional differences between the different observationally based estimates of new production and uncertainties in the remineralization scheme, it is probably unwise to stretch the numerical comparisons between models and observational estimates too far. As can be seen by looking at Fig. 3, much of the uncertainty in computing the new production arises from how to parameterize the effect of temperature, which is itself a function of latitude. It is certainly possible, for example, that some of the differences between the observational estimates and models arises from systematic regional biases in the methods used to estimate new production. On the other hand, it is also possible that certain differences arise from biases in the model—especially as regards the way in which new production is calculated. The following section considers three regions where there are significant differences amongst the observational and model estimates, namely the equatorial zone, the North Atlantic, and the North Pacific.

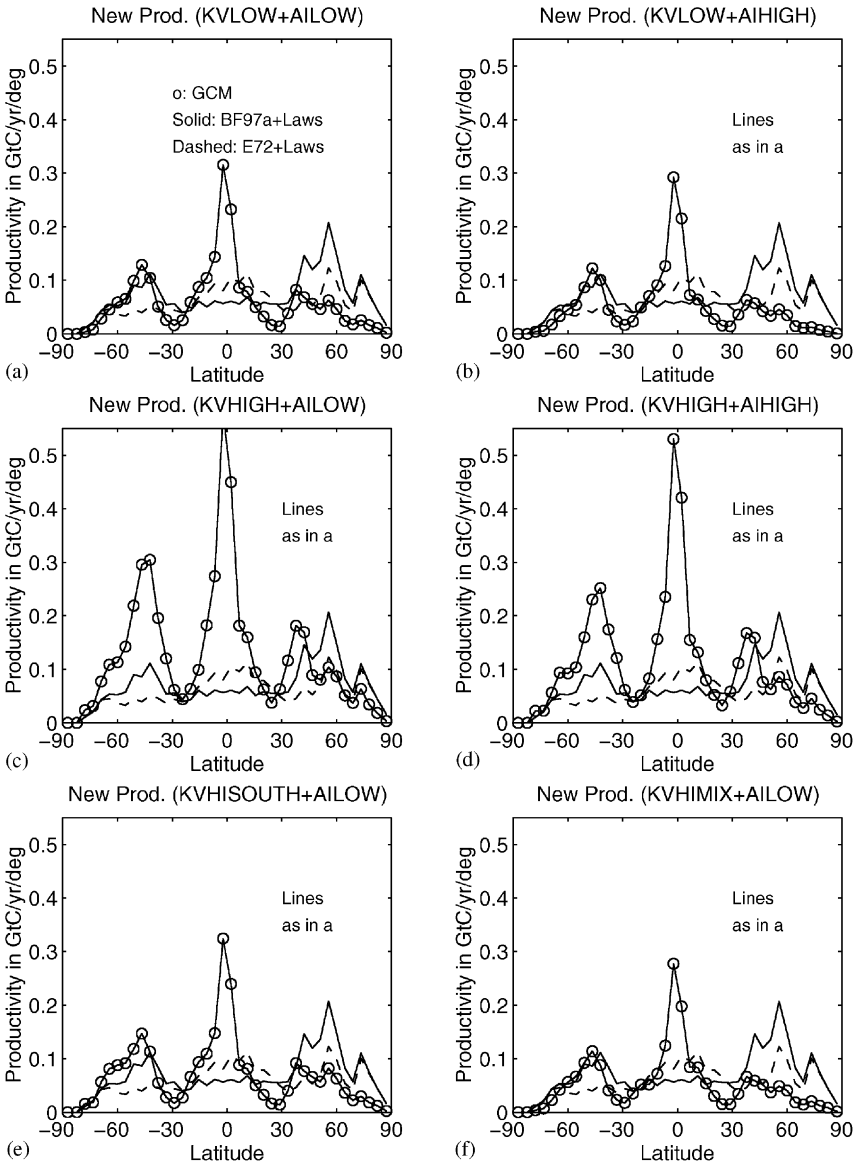

Fig. 16. Productivity in the 6 GCMs (○), compared with that inferred from satellite using BF97 a (solid line) and E72 (dashed line). (a) KVLOW + AILOW (b) KVLOW + AIHIGH (c) KVHIGH + AILOW (d) KVHIGH + AIHIGH. (e) KVHISOUTH + AILOW (f) KVHIMIX + AILOW.

6. Regional differences

6.1. Why are the models higher than the observational estimates in the equatorial zone?

One of the intriguing issues raised by this comparison is the difference in the magnitude and pattern of low-latitude new production between the models and the two satellite estimates. The

BF97a parameterization for P^B_{opt} shows relatively little structure in the low latitudes, while the models and the E72 parameterization show an export production that is systematically higher in upwelling zones and lower in downwelling zones. As seen in Fig. 3b, the primary production in low latitudes has little latitudinal dependence when the BF97a algorithm is used.

One area which may be particularly important is the Eastern Equatorial Pacific (the so-called "cold tongue" region from 5S–5N and 180W–90W). The biology of this region has been intensively studied over the past decades, including during the JGOFS Equatorial Pacific (EqPac) process study. The cold tongue is one of the most important areas for new production in the numerical models. The KVLOW + AILOW model predicts a new production of 1.6 GtC yr^{-1} while the KVHIGH + AIHIGH model predicts 2.8 GtC yr^{-1}. This amounts to one-third of the total tropical new production and 15% of the global new production in both models. By contrast, the export production in the Eastern Equatorial Pacific predicted by both BF97a + Laws (0.13 GtC yr^{-1}) and E72 + Laws (0.16 GtC yr^{-1}) is a great deal smaller than either of these numbers.

A large number of estimates for new production within the cold tongue have been made. Chavez and Barber (1987) made two estimates—one based on the rate of nutrient transport into the mixed layer implied by the rate of upwelling (1.9 GtC yr^{-1}), the other based on an estimate of f-ratio at 0.4 and primary production (0.84 GtC yr^{-1}). These estimates are much higher than those made using satellite color. However, there appear to be significant problems with the highest number, in that a significant amount of the upwelled nutrient is advected out of the the cold tongue in the surface layer (Chai et al., 1996). A large number of estimates of new production were made as part of the EqPac experiment. Ku et al. (1995) used the ^{228}Ra budget in the euphotic zone to estimate a new production of 0.8 GtC yr^{-1}. McCarthy et al. (1996) used direct measurements of nitrogen uptake during EqPac to estimate a new production of 0.8 GtC yr^{-1} and a primary production of around 7 GtC yr^{-1}. The latter number is in agreement with the observations of Barber et al. (1996) who estimate a primary production of 8 GtC yr^{-1} based on the EqPac transects. Murray et al. (1996) have a smaller estimate of export production (0.47 GtC yr^{-1}) but this is still significantly larger than the satellite-based estimates.

Several numerical models with reasonably high resolution have been used to estimate new production within the cold tongue. Toggweiler and Carson (1995) used a high resolution model of the tropical Pacific coupled with the ecosystem model of Fasham et al. (1990). They were able to match observed nitrate distributions with a new production of 1.0 GtC yr^{-1}. Chai et al. (1996) used a similar model to estimate a new production of 0.7–0.8 GtC yr^{-1}. Aumont et al. (1999) using a semi-diagnostic model estimated a new production from 4.7S–4.7S and 130W to 80W (about half the area of the cold tongue) of 0.5 GtC yr^{-1}. The consensus from these high-resolution models and in-situ data appears to be that the coarse-resolution GCMs produce too large a value for new production, while the satellite-based estimates are too low.

The satellite-based estimates could be too low either because of an underestimate of the primary production, or an underestimate of the f-ratio. Comparison with the results of the EqPac experiment suggest the former explanation. Barber et al. (1996) estimate the true primary production within the cold tongue to be around 75 mmol C m^{-2} day^{-1}, implying a total production of 8.2 GtC yr^{-1}. The satellite-based estimates are much lower, 1.2 GtC yr^{-1} for BF97a and 1.7 GtC yr^{-1} for E72. Apparently the satellites miss a significant portion of the new production in the Eastern Equatorial Pacific. Some part of this is likely due to the underestimate

of chlorophyll in CZCS. Values of chlorophyll within the cold tongue are around 0.1 mg m^{-3} while the measurements of Barber et al. (1996) are higher by a factor of 2–3. It is also possible that the algorithms used to scale chlorophyll to production fail to account for the fact that a large fraction of the production in the Equatorial Pacific occurs at significant depths (> 40 m).

Why do the GCMs predict such high values of new production in the Equatorial Pacific? An obvious answer is that something is wrong either with the circulation or the biological cycling, but what? High production in a region may result from a number of causes. The first is that the flow of nutrients through the region is too large. If the circulation within the GCM brings too much nutrient from the deep ocean into the tropical pycnocline, this nutrient will drive overly high production. The range of models presented here gives a hint about what one such problem with the transport could be, namely that the effective mixing coefficient in the KVLOW + AILOW case is still too high. It is well known that advection schemes can produce numerical diffusivity (see Oschlies (2000) for a discussion of this phenomenon in an eddy-permitting model). These errors become smaller as the vertical resolution becomes finer. It is quite likely that the relatively coarse vertical resolution in the current model results in adding some numerical diffusion to the explicit vertical diffusion. As noted above, this would result in excessive upwelling of deep water into the tropical thermocline, resulting in overly high new production.

A second possibility, however, is that model circulation results in too efficient a retention of nutrients with the tropics. An example of this is the well-known phenomenon of "nutrient trapping" (Najjar et al., 1992; Aumont et al., 1999). Nutrient trapping arises when water upwelled into the surface layer passes through the region where the majority of remineralization occurs. The nutrients stripped from the surface waters by biological cycling then get added to the upwelled water, with the result that very high concentrations of nutrients build up in the upwelled water and excessively high new production is found at the surface. Aumont et al. (1999) suggested that coarse models such as those used in this study would produce nutrient trapping near the equator as a result of low horizontal resolution. Their argument is that when the resolution is low, the water upwelling into the equatorial surface layer contains a higher fraction of nutrient-rich intermediate water relative to the relatively low-nutrient water associated with the equatorial undercurrent.

In order to evaluate whether lateral transport or retention of nutrients was most important in maintaining high productivity in the Eastern Equatorial Pacific, we examined the water and phosphate budget along the equator using regions as similar as possible to those in Aumont et al. (1999). Despite the lack of resolution in the undercurrent region (resulting in a current that was extremely slow and spread out) the total water flux associated with the current in the Eastern Equatorial Pacific (130W–80W, 5N–5S, for which water and phosphate budgets are shown in Fig. 17c and d) was not too dissimilar to Aumont et al. (1999) (compare with their Figs. 4 and 7). For example, the total upwelling across 50 m was 24.4 Sv in the KVLOW + AILOW model, quite similar to the 23.1 Sv in the standard case of Aumont et al. (1999). As a result, the total supply of nutrients to the top 50 m, and the total production associated with this region produced by model KVLOW+AILOW (Fig. 17c) is very similar to their baseline case. Most of the nutrients supplied to the upper 50 m are transported into the region laterally (76%), with only 20% being supplied by remineralization. Retention of nutrients within the Equatorial Pacific explains only a small fraction of the high values of new production.

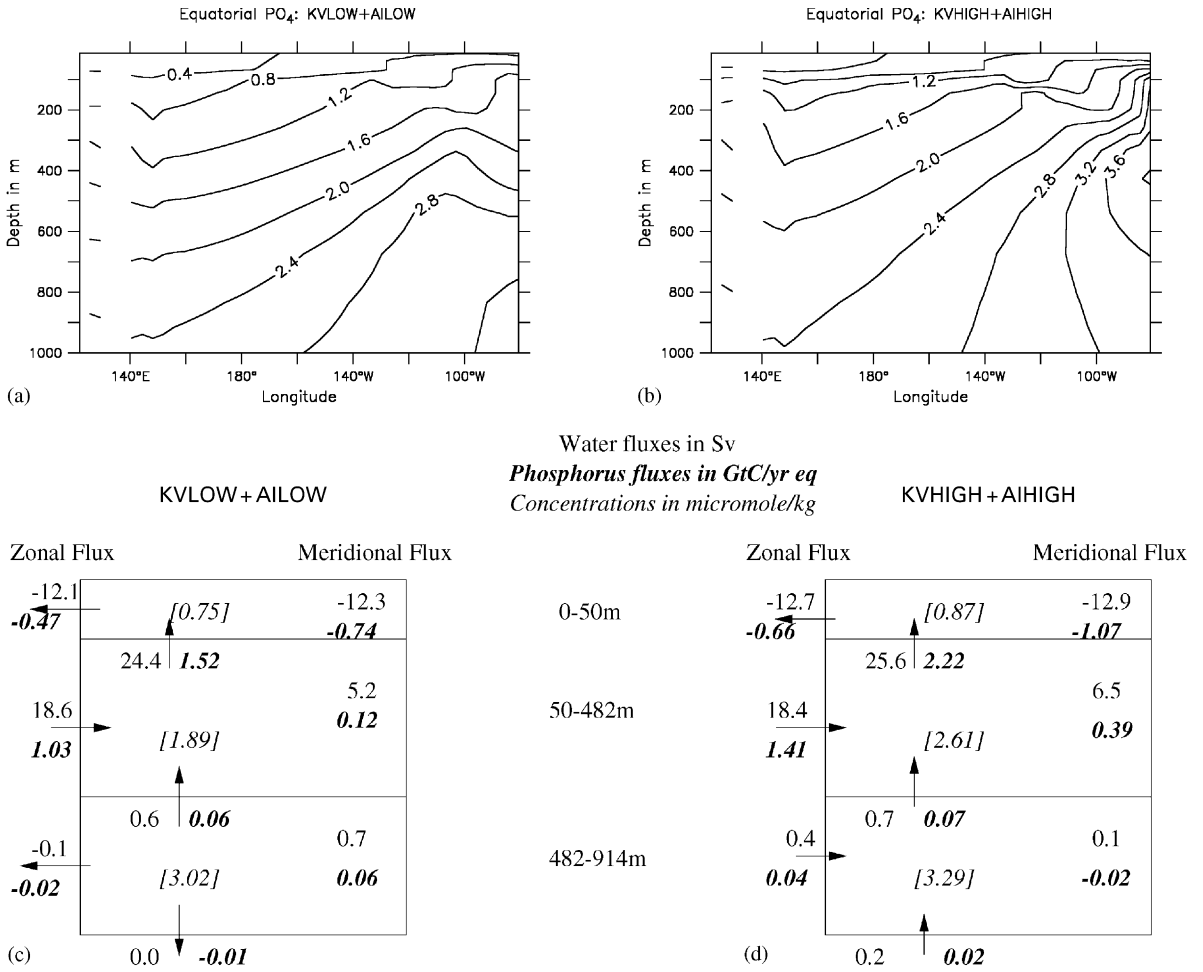

Fig. 17. Nutrient and water budget in the Equatorial Pacific. (a) PO_4 concentrations along the equator, model KVLOW + AILOW. (b) PO_4 concentrations along the equator, KVHIGH + AIHIGH. (c) Schematic of the water and nutrient budget from 130W to 80W and 5N to 5S for run KVLOW + AILOW. Regular type denotes water fluxes in Sv, *bold italics* are phosphate fluxes (PO_4 + DOP) scaled to units of GtC yr^{-1}, bracketed *italics* show average concentrations of PO_4. Biological uptake and remineralization are not shown, so phosphate transport numbers will not add up to zero within boxes. (d) Same as (c) for run KVHIGH + AIHIGH.

The picture does not change substantially for the KVHIGH + AIHIGH simulation. Increasing the vertical diffusion coefficient does result in (Fig. 17b, d) higher concentrations appearing in the Eastern Equatorial Pacific. However, 81% of the nutrients supplied to the surface layer come from lateral transport. If nutrient trapping were important in explaining the difference between KVLOW+AILOW and KVHIGH+AIHIGH, the lateral transport would be less important and remineralization more important in the latter simulation. In fact, the reverse is true.

What then are we to make of the high nutrient concentrations in KVHIGH+AIHIGH? Examination of the water budget for the lower boxes in Fig. 17c and d shows that the water along

the coast of South America is essentially stagnant in comparison with the surface waters above it. It is quite sensitive to changes in the local flux of nutrients and can easily become enriched in nutrients. This does not mean, however, that it plays any significant role in setting the biological productivity at the surface. In neither of the cases shown in Fig. 17 is the vertical transport of nutrients across 482 m a major contributor to the nutrient balance (accounting for only a few percent of the nutrients transported across 50 m). The fact that excessively high nutrients are found in the Eastern Equatorial Pacific in certain versions of our model is a result, but *not* a cause of high productivity.

6.2. Why are the observational estimates so different in the North Atlantic?

The region with the largest difference between the different observational estimates of new production is the subpolar North Atlantic (Table 1, penultimate column). The differences seen in this column do not disappear when smaller areas are considered. The LN2000 phosphate estimate produces an extremely low value of carbon flux in the North Atlantic between 40N and 66N (0.34 GtC yr^{-1}), while the BF97a+Laws estimate is 1.9 GtC yr^{-1} in this same area. A more detailed analysis shows that a large fraction of this production estimated from satellite color (0.86 GtC) occurs during the months of June, July, and August. Over the entire North Atlantic north of 40N the BF97a+Laws production is 3.3 GtC yr^{-1} (Table 1, penultimate column) with 1.65 GtC occurring during June, July and August. The circulation models all lie in between the extreme estimates of the phosphate-based production and the BF97a+Laws production.

A value of 0.8 GtC yr^{-1} for new production during the summer months over the North Atlantic between 40N and 66N would require a drawdown of 0.5 μmol/kg phosphate if the drawdown were in Redfield ratio. This is supported by the measurements of Takahashi et al. (1993) at the NABE site, showing a maximum concentration of around 0.6 μmol/kg and a minimum concentration of about 0.1. The oxygen-based measurements of Najjar and Keeling (2000) produce an estimate of new production in the Subpolar North Atlantic of about 0.8 GtC yr^{-1}, again consistent with a somewhat larger seasonal production. However, LN2000 by contrast shows a drawdown of only about 0.2 μmol/kg on average in this region. The drawdown of nitrate was essentially in Redfield ratio with that of phosphate in all of the measurement programs, so that it is unlikely that nitrogen fixation played a major role in accounting for the difference between the oxygen and phosphate-based estimates.

Some of the differences between the nutrient climatology and the models can be accounted for by the methodology used by LN2000. In order to reduce the effects of measurement errors on the estimate of seasonal production, they estimated new production from the difference between the averaged January–March nutrient concentration and the averaged July–September nutrient concentration. As can be seen in Fig. 18 in the Subpolar North Atlantic, the maximum surface phosphate does not appear until March, as this is the month where the deepest convection occurs. Concentrations in January and February are substantially lower than in March, lowering the estimate of maximum phosphate concentration. Similarly, there is a substantial drawdown of nutrients in the late summer, so that about half the annual range occurs between August and September. This means that a seasonal average will raise the estimate of the minimum phosphate concentration. When the annual range is computed using monthly rather than seasonal data, the

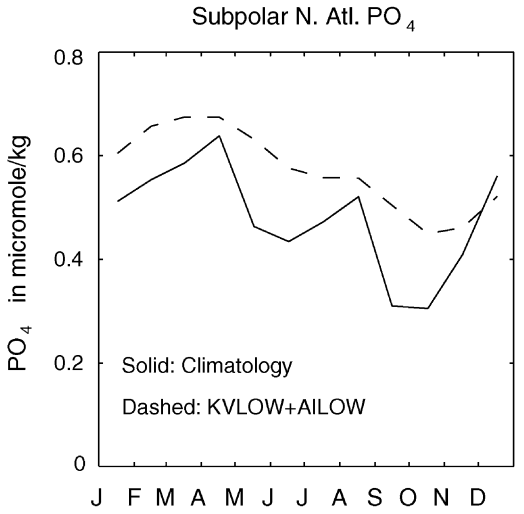

Fig. 18. Annual cycle of phosphate in the subpolar North Atlantic (40N–66N) from data (solid line) of Louanchi and Najjar (in press) and model KVLOW + AILOW. The modelled phosphate is higher as a result of the parameterization of production in terms of restoring.

average for the northern North Atlantic is 0.43 μmol/kg and the total seasonal production increases to 0.6 GtC yr^{-1}.

Reconciling the two satellite-based estimates of primary production is somewhat harder. It is possible that some of the difference arises because of biases in the data set that was used to create the BF97a P^B_{opt} curve. Examination of this curve shows high values of P^B_{opt} (larger than 10) occurring almost exclusively in coastal zones where relatively cold waters are brought to the surface. It is not clear whether the values from such regions should apply to the open waters of the North Atlantic. For the satellite-based estimates to serve as a useful constraint on the circulation in the North Atlantic, it is imperative that this issue be resolved.

6.3. *Why are the model predictions so low in the North Pacific?*

A region where the models all disagree with the observational estimates of new production is the subpolar North Pacific (Table 1, last column). All of the observational estimates of new production are relatively high in this region, ranging from 0.6 to 1.5 GtC yr^{-1}. The lower value is still substantially higher, however, than the highest model value (the models range from 0.2 to 0.3 GtC yr^{-1}). Since the models are all forced by restoring to the nutrient climatology it is not obvious why they should substantially underpredict the total productivity. Recent comparisons as part of the OCMIP project (F. Louanchi, pers. comm.) reveal this to be a problem with a number of general circulation models.

Examination of the nutrient cycle in the North Pacific reveals part of the problem. As shown in Fig. 19a, the observed surface nutrient cycle over the North Pacific exhibits a strong annual cycle. The wintertime maximum of this cycle is not properly captured by the numerical model, resulting in a gross underestimate of the new production. The question then arises, is this failure to produce

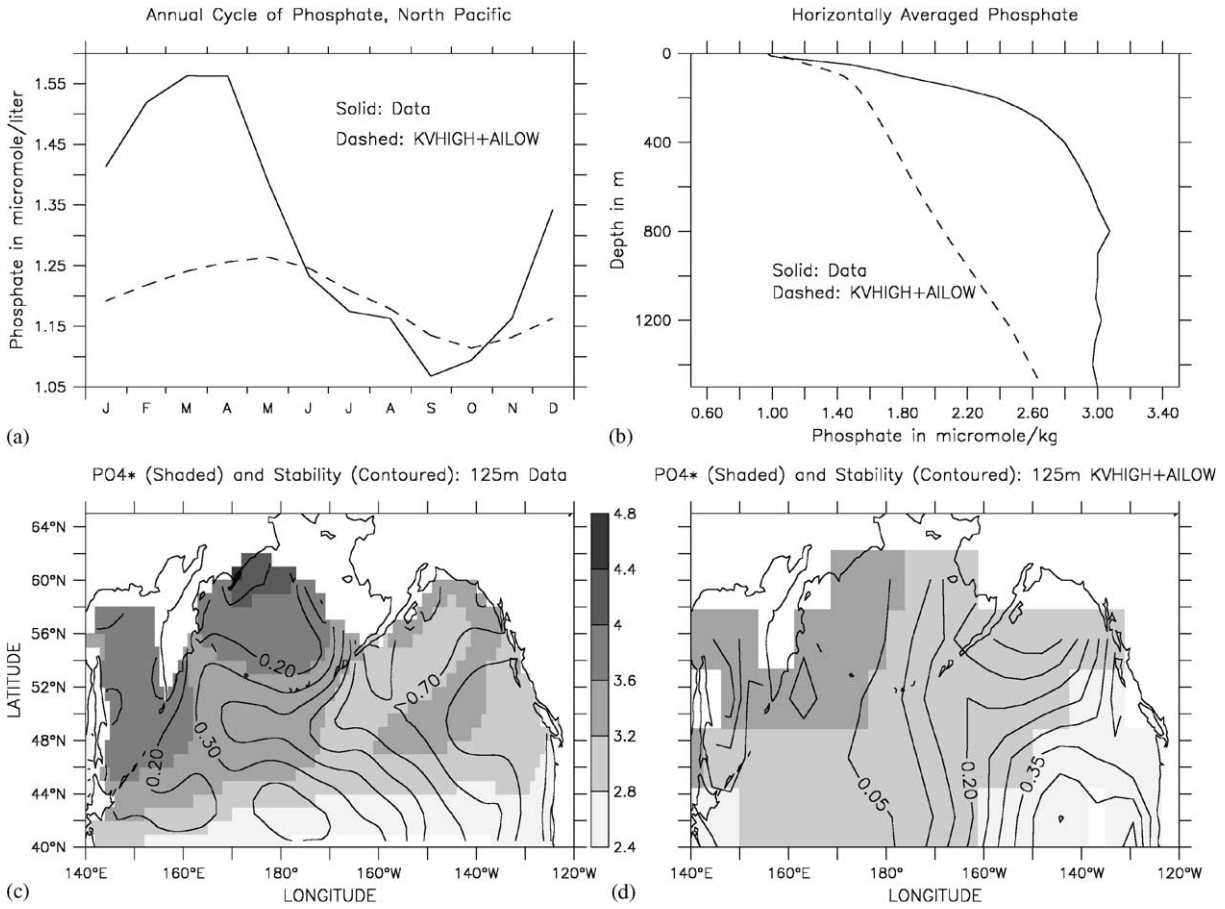

Fig. 19. Nutrients and density in the North Pacific. (a) PO_4 from the climatology of LN2000 with which the model is forced, and averaged PO_4 over the North Pacific from model KVHIGH + AILOW (chosen as having the highest new production). Note the failure to bring up nutrients during the wintertime in this model. (b) Horizontally averaged phosphate in the North Pacific. Note the deficit in modelled phosphate at depths from 100–1200 m. (c) PO_4^* (phosphate + oxygen/170) at 125 m is shaded and density difference between 150 and 85 m is contoured using data. (d) Same as (c) for the model.

high nutrients during the wintertime the fault of the model to mix up nutrients from sufficient depth, or is it that the water mass which is being mixed up has insufficient nutrients?

There has been some speculation (R.M. Key, pers. comm.) that the relationship between radiocarbon and silicate requires the existence of strong vertical mixing somewhere in the North Pacific. It is possible that relatively low temporal resolution in the forcing and low spatial resolution in the model grid results in the dynamics of wintertime mixing in the North Pacific being poorly simulated. Initial comparisons with a model that included a more sophisticated boundary layer (S. Doney, pers. comm.) show that such a scheme is not by itself sufficient to resolve the problem of low nutrient transport into the mixed layer; however, the differences may only be resolvable at higher resolution. Interestingly, however, Archer et al. (1993) also found that

a one-dimensional balance was insufficient to explain both the cycle of nutrients and density at station PAPA. Denman and Pena (1999) found it necessary to add nutrients to the mixed-layer base in order to keep sinking detritus from removing too much nutrient.

The general circulation models also have trouble keeping enough phosphate in the waters immediately below the pycnocline. As shown in Fig. 19b, which compares the horizontally averaged phosphate profile from model KVHIGH+AILOW and data, the model significantly underpredicts the phosphate concentration between depths of 100 and 1500 m. Model KVHIGH+AILOW was chosen for this comparison because it had the highest new production of any of the simulations. There are two possible reasons why the modelled phosphate might be low. The first possibility is that the real North Pacific is a place where nutrient trapping does occur, but that the model fails to capture this because vertical exchange is too slow relative to horizontal exchange. If this were true, the problem would be that the rate at which phosphate is recycled in the upper intermediate waters of the North Pacific would be too slow in the models. A second possibility is that the model circulation does not feed high-nutrient intermediate waters into the North Pacific. If this were true, the low new production over most of the North Pacific would result from an insufficient lateral supply of high-phosphate water.

To examine which of these processes is most likely to explain the situation in the North Pacific, it is necessary to consider a watermass tracer in which the effects of nutrient cycling have been removed. One such tracer is $PO_4^* = PO_4 + O_2/170$, which is conserved outside the mixed layer with respect to remineralization of organic matter (Broecker et al., 1985). High values of PO_4^* are found when nutrient-rich water is brought to the surface ocean, oxygen is added, but nutrients are not stripped out of the water. If phosphate concentrations in the upper North Pacific thermocline are low, but PO_4^* is correct, this would indicate that the phosphate deficit arises from insufficient addition of remineralized phosphate to these waters. If on the other hand, the phosphate and PO_4^* are both low by the same amount, the implication would be that some water mass that is formed containing relatively high values of phosphate in the real ocean is not being formed in the model.

The shading in Fig. 19c shows PO_4^* in the North Pacific at 125 m from the Levitus 1994 data set. The contours show the density difference in kg m^{-3} between 85 and 150 m in this data set. The data clearly show a patch of water with very high PO_4^*, which seems to form along the continental margin of Asia and along the Aleutians in a region where the stratification, though lower than elsewhere in the North Pacific, is still significant. The model (Fig. 19d) fails to capture this water mass, despite the fact that the stratification over this depth range is very weak. The high PO_4^* water is associated with a potential density of 26.6. In the Levitus data set, this water is not found at the surface along the northern boundary of the North Pacific. As a result, the lateral supply of nutrients to the upper North Pacific Ocean is far weaker than it should be. PO_4^* concentrations in the model are lower than in the data by around 0.2–0.4 μmol l^{-1}, so that this failure to supply high-nutrient intermediate water could account for approximately half of the phosphate deficit in Fig. 19b.

7. Conclusions

Models with different physics can produce similar pycnoclines, but very different nutrient cycles. As a result, measurements of nutrient cycling can give information about model physics

complementing that provided by the large-scale density structure and transient tracers. Estimates of new production generally support a physical picture in which vertical diffusion is weak within the low latitude pycnocline, (although at present the accuracy of the measurements used to produce such estimates remains questionable). Within such a physical picture, relatively little deep water upwells through the low-latitude pycnocline. This is inconsistent with high values of vertical diffusion advocated by certain authors (Marotzke, 1997; Gibson, 1999) and seen in some circulation models that have strong equatorial upwelling. However, it is consistent with the picture emerging from microstructure and tracer release measurements (Ledwell et al., 1993, 1998; Polzin, 1999).

In general, insofar as the remineralization of organic matter occurs at relatively shallow depths, the results presented here support a picture of ocean circulation where the vertical exchange is relatively weak away from the polar regions. This has implications for the wider field of oceanography and climate dynamics insofar as it supports a picture of the circulation in which vertical exchange is largely mediated through the Southern Ocean, as suggested by Toggweiler and Samuels (1998), Gnanadesikan (1999a) and Hirst (1999). This has important implications for how climate and global biogeochemistry can be driven by the atmosphere. If the majority of vertical exchange were to occur through the low latitudes, it would be thought that the most important processes for determining global density and nutrient structure would be those in the North Atlantic Ocean, where the primary transformation of light to dense water occurs. By contrast, if the Southern Ocean is the primary zone of upwelling changes in the Southern Ocean winds could be important as well.

However, this work also demonstrates that the conceptual picture of ocean circulation depicted in Fig. 1 is too simple. It does not capture the important fact that convection (as distinguished from the large-scale advective circulations shown in Figs. 1 and 7) plays a key role in supplying nutrients to the high-latitude surface oceans, and that this convective supply is also strongly affected by vertical and lateral diffusion. Additionally, the theory does not include the formation of deep-water within the Southern Ocean. While the rates of convection and deep-water formation within the Southern Ocean have a relatively small effect on the globally integrated new production, they could be important for other biogeochemical processes. For example, Sarmiento and Toggweiler (1984) note that the rate of exchange between the high surface latitudes and deep ocean plays a critical role in determining the atmospheric pCO_2. Toggweiler (1999) recently proposed that changes in the rate of convection within the Southern Ocean are responsible for driving glacial–interglacial changes in atmospheric carbon dioxide. The initial analysis of a set of model runs based on those described here supports the idea that the rate of convection within the Southern Ocean determines the extent to which the full solubility and biological pumps of carbon are realized in the modern ocean, as well as determining the ability of nutrient depletion to draw down atmospheric carbon dioxide.

There are still major discrepancies on regional scales regarding the magnitude of new production, representing major opportunities for research. In some regions, such as the tropical Pacific, there are clear questions regarding the satellite estimates of new production. Convection plays a relatively minor role in the equatorial nutrient supply, and the Ekman transport is known reasonably well. Hydrographic estimates of the production in the Pacific (Chavez and Barber, 1987) based on this physical picture, as well as a range of model estimates predict relatively high values of new production in this region relative to the satellites. This suggests that the satellite-

based estimates of new production should be carefully scrutinized in the equatorial region. Somewhat surprisingly, there also remain major differences in the estimates of seasonal variation and mean production in the North Atlantic, despite a large body of observational work there. The resolution of this question should be pursued both by better estimates of what regulates P^B_{opt} (in investigating the role of iron and nutrient supply) and by careful validation of satellite estimates of production in this critical area. In the North Pacific, all of the models have levels of new production that are far too low. It seems likely that this is due to the formation of a high phosphate water mass along the coast of Asia which is not captured in the numerical model. Better studies to quantify the sources of nutrients to the North Pacific mixed layer and to characterize the fate of organic matter produced within the mixed layer would significantly improve our understanding of this region.

Acknowledgements

The authors thank Robbie Toggweiler, Paul Falkowski, Mike Behrenfeld, Ferial Louanchi, Ray Najjar, Scott Doney and an anonymous reviewer for useful comments on this work. This work was supported by the Carbon Modeling Consortium (NOAA Grant NA56GP0439).

References

Anderson, L.A., Sarmiento, J.L., 1995. Global ocean phosphate and oxygen simulations. Global Biogeochemical Cycles 9, 621–636.

Antoine, D., Morel, A., 1996. Oceanic primary production. 1. Application of a spectral light-photosynthesis model in view of application to satellite chlorophyll observations. Global Biogeochemical Cycles 10, 43–55.

Archer, D., Emerson, S., Powell, T., Wong, C.S., 1993. Numerical hindcasting of sea surface pCO_2 at Weathership Station Papa. Progress in Oceanography 32, 319–351.

Aumont, O., Orr, J.C., Monfray, P., Madec, G., Maier-Reimer, E., 1999. Nutrient trapping in the equatorial Pacific: The ocean circulation solution. Global Biogeochemical Cycles 13, 351–369.

Barber, R.T., Sanderson, M.P., Lindley, S.T., Chai, F., Newton, J., Trees, C.C., Foley, D.G., Chavez, F.P., 1996. Primary productivity and its regulation in the eastern equatorial Pacific during and following the 1991–1992 El Nino. Deep Sea Research II 43, 933–969.

Behrenfeld, M.J., Falkowski, P.G., 1997a. Photosynthetic rates derived from satellite-based chlorophyll concentration. Limnology and Oceanography 42, 1–20.

Behrenfeld, M.J., Falkowski, P.G., 1997b. A consumer's guide to phytoplankton primary productivity models. Limnology and Oceanography 42, 1479–1491.

Broecker, W.S., Takahashi, T., Takahashi, T., 1985. Sources and flow patterns of deep ocean waters as deduced from potential temperature, salinity, and initial phosphate calculations. Journal of Geophysical Research 90, 6925–6939.

Bryan, F.O., 1987. Parameter sensitivity studies of primitive equation ocean general circulation models. Journal of Physical Oceanography 17, 970–985.

Bryan, K., Lewis, L.J., 1979. A water mass model of the world ocean. Journal of Geophysical Research 84, 2503–2517.

Chai, F., Lindley, S.T., Barber, R.T., 1996. Origin and maintenance of a high nitrate condition in the equatorial Pacific. Deep Sea Research II 43, 1031–1064.

Chavez, F.P., Barber, R.T., 1987. An estimate of new production in the Equatorial Pacific. Deep Sea Research 34, 1229–1243.

Chavez, F.P., Toggweiler, J.R., 1995. Physical estimates of global new production: The upwelling contribution. In: Summerhayes, C.P., Emeis, K.-C., Angel, M.V., Smith, R.L., Zeitschel, B. (Eds.), Upwelling in the Ocean: Modern Processes and Ancient Records.. Wiley, New York, pp. 313–320.

Conkright, M.E., Levitus, S., Boyer, T.P., 1994. World Ocean Atlas, 1994, Volume 1: Nutrients, NOAA Atlas NESDIS 1, U.S. Department of Commerce, Washington, D.C.

da Silva, A., Young, A.C., Levitus, S., 1994. Atlas of Surface Marine Data 1994, Volume 1: Algorithms and Procedures. NOAA Atlas NESDIS 6, U.S. Department of Commerce, Washington, D.C.

Denman, K.L., Pena, M.A., 1999. A coupled 1-D physical-biological model of the northeast subarctic Pacific Ocean with iron limitation. Deep Sea Research II 46, 2877–2908.

Dugdale, R.C., Goering, J.J., 1967. Uptake of new and regenerated forms of nitrogen in primary productivity. Limnology and Oceanography 12, 196–206.

Dutay, J.-C., Bullister, J.L., Doney S.C., Orr, J.C., Najjar, R., Caldeira, K., Champin, J.-M., Drange, H., Follows, M., Gao, Y., Gruber, N., Hecht, M.W., Ishida, A., Joos, F., Lindsay, K., Madec, G., Maier-Reimer, E., Marshall, J.C., Matear, R.J., Monfray, P., Plattner, G.-K., Sarmiento, J., Schlitzer, R., Slater, R., Totterdell, I.J., Weirig, M.-F., Yamanaka, Y., Yool, A., 2001. Evaluation of ocean model ventilation with CFC-11: comparison of 13 global ocean models. Ocean Modelling, in press.

Eppley, R.W., 1972. Temperature and phytoplankton growth in the sea. Fisheries Bulletin 70, 1063–1084.

Eppley, R.W., Peterson, B.J., 1979. Particulate organic matter flux and planktonic new production in the deep ocean. Nature 282, 677–680.

Fasham, M.J.R., Ducklow, H.W., McKelvie, S.M., 1990. A nitrogen-based model of plankton dynamics in the oceanic mixed layer. Journal of Marine Research 48, 591–639.

Feldman, G.C., Kuring, N.A., Ng, C., Esaias, W.E., McClain, C.R., Elrod, J.A., Maynard, N., Endres, D., Evans, R., Brown, J., Walsh, S., Carle, M., Podesta, G., 1989. Ocean Color: Availability of the Global Data Set. EOS 70, 634–641.

Gent, P., McWilliams, J.C., 1990. Isopycnal mixing in ocean circulation models. Journal of Physical Oceanography 20, 150–155.

Gent, P., Willebrand, J., McDougall, T.J., McWilliams, J.C., 1995. Parameterizing eddy-induced transports in ocean circulation models. Journal of Physical Oceanography 25, 463–474.

Gibson, C.H., 1999. Fossil turbulence revisited. Journal of Marine Systems 21, 147–167.

Gnanadesikan, A., 1999a. A simple theory for the structure of the oceanic pycnocline. Science 283, 2077–2079.

Gnanadesikan, A., 1999b. A global model of silicon cycling: Sensitivity to eddy parameterization and dissolution. Global Biogeochemical Cycles 13, 199–220.

Gnanadesikan, A., 1999c. Numerical issues for coupling biological models with isopycnal mixing schemes. Ocean Modelling 1, i 1–15.

Gnanadesikan, A., Toggweiler, J.R., 1999. Constraints placed by silicon cycling on vertical exchange in general circulation models. Geophysical Research Letters 26, 1865–1868.

Gnanadesikan, A., Weller, R.A., 1995. Structure and instability of the Ekman layer in the presence of surface gravity waves. Journal of Physical Oceanography 25, 3148–3171.

Griffies, S.M., 1998. The Gent–McWilliams skew flux. Journal of Physical Oceanography 28, 831–841.

Griffies, S.M., Gnanadesikan, A., Larichev, V.D., Pacanowski, R.C., Dukowicz, J.K., Smith, R.D., 1998. Isoneutral diffusion in a z-coordinate ocean model. Journal of Physical Oceanography 28, 805–830.

Griffies, S.M., Pacanowski, R.C., Hallberg, R.W., 2000. Spurious diapycnal mixing associated with advection in a z-coordinate ocean model. Monthly Weather Review 128, 538–564.

Held, I., Larichev, V.D., 1996. A scaling theory for horizontally homogeneous baroclinically unstable flow on a beta-plane. Journal of the Atmospheric Sciences 53, 946–952.

Hellerman, S., Rosenstein, M., 1983. Normal monthly wind stress over the World Ocean with error estimates. Journal of Physical Oceanography 13, 1093–1104.

Hirst, A.C., 1999. Determination of water component age in ocean models: Application to the fate of North Atlantic Deep Water. Ocean Modelling 1, 81–94.

Huang, R.X., 1999. Mixing and energetics of the Oceanic thermohaline circulation. Journal of Physical Oceanography 29, 727–746.

Hughes, T.M.C., Weaver, A., 1994. Multiple equilibria of an asymmetric, two-basin ocean model. Journal of Physical Oceanography 24, 619–637.

Johnson, G.C., Warren, B.A., Olson, D.B., 1991. Flow of bottom water in the Somali Basin. Deep Sea Research 38, 637–652.

Ku, T.L., Luo, S., Kusakabe, M., Bishop, J.K.B., 1995. ^{228}Ra-derived nutrient budgets in the upper equatorial Pacific and the role of "new" silicate in limiting productivity. Deep Sea Research II 42, 479–497.

Laws, E.A., Falkowski, P., Carpenter, E.A., Ducklow, H., 2000. Temperature-dependence of the f-ratio. Global Biogeochemical Cycles 14, 1231–1246.

Ledwell, J.R., Watson, A.J., Law, C.S., 1993. Evidence for slow mixing across the pycnocline from an open-ocean tracer release experiment. Nature 364, 701–703.

Ledwell, J.R., Watson, A.J., Law, C.S., 1998. Mixing of a tracer in the pycnocline. Journal of Geophysical Research 103, 21499–21529.

Levitus, S., Boyer, T., 1994. World Ocean Atlas 1994 Volume 4: Temperature, NOAA Atlas NESDIS 4, U.S. Department of Commerce, Washington D.C., 1994.

Lilover, M.J., Lozvatsky, I.D., Gibson, C.H., Nabatov, V., 1993. Turbulent exchange through the equatorial undercurrent core of the Central Pacific. Journal of Marine Systems 4, 183–195.

Louanchi, F., Najjar, R.G., 2000. A global climatology of phosphate, nitrate and silicate in the upper ocean: Spring–summer production and shallow remineralization. Global Biogeochemical Cycles 14, 957–977.

Marotzke, J., 1997. Boundary mixing and the dynamics of three-dimensional thermohaline circulations. Journal of Physical Oceanography 27, 1713–1728.

Martin, J.H., Knauer, G.A., Karl, D.M., Broenkow, W.W., 1987. VERTEX: Carbon cycling in the Northeast Pacific. Deep Sea Research 34, 267–285.

Murnane, R., Sarmiento, J.L., Le Quere, C., 1999. Spatial distribution of air-sea CO_2 fluxes and the interhemispheric transport of carbon by the oceans. Global Biogeochemical Cycles 13, 287–305.

Murray, J.W., Young, J., Newton, J., Dunne, J., Chapin, T., Paul, B., McCarthy, J.J., 1996. Export flux of particulate organic carbon from the central equatorial Pacific determined using a combined drifting trap-^{234}Th approach. Deep Sea Research II 43, 1095–1132.

McCarthy, J.J., Garside, C., Nevins, J.L., Barber, R.T., 1996. New production along 140W in the equatorial Pacific during and following the 1992 El Nino event. Deep Sea Research II 43, 1065–1093.

Najjar, R.G., 1990. Simulations of the phosphorus and oxygen cycles in the world ocean using a general circulation model. Ph.D. Thesis. Princeton University, Princeton, NJ.

Najjar, R.G., Keeling, R.F., 2000. The mean annual cycle of the air-sea oxygen flux: a global view. Global Biogeochemical Cycles 14, 573–584.

Najjar, R.G., Orr, J.C., 1998. Design of OCMIP 2 simulations of chloroflourocarbons, the solubility pump and common biogeochemistry, unpublished manuscript. available at /www.ipsl.jussieu.fr/OCMIP/.

Najjar, R.G., Sarmiento, J.L., Toggweiler, J.R., 1992. Downward transport and fate of organic matter in the ocean: Simulations with a general circulation model. Global Biogeochemical Cycles 6, 45–76.

Oschlies, A., 2000. Equatorial nutrient trapping in biogeochemical ocean models: The role of advection numerics. Global Biogeochemical Cycles 14, 655–667.

Pacanowski, R.C., Griffies, S.M., 1999. The MOM 3 Manual, Alpha Version, NOAA/Geophysical Fluid Dynamics Laboratory, 580 pp.

Park, Y.-G., Bryan, K., 2000. Comparison of thermally-driven circulations from a depth-coordinate model and an isopycnal-layer model, Part I: Scaling-law sensitivity to vertical diffusivity. Journal of Physical Oceanography 30, 590–605.

Peters, H., Gregg, M.C., Toole, J.M., 1988. On the parameterization of equatorial turbulence. Journal of Geophysical Research 93, 1199–1218.

Polzin, K.L., 1999. A rough recipe for the energy balance of quasi-steady interal lee waves. 'Aha Huliko'a: Dynamics of oceanic internal gravity waves II, pp. 117–128.

Polzin, K.L., Toole, J.M., Ledwell, J.R., Schmitt, R.W., 1997. Spatial variability of turbulent mixing in the abyssal ocean. Science 276, 93–96.

Price, J.F., Sundermeyer, M.A., 1999. Stratified Ekman layers. Journal of Geophysical Research 104, 20467–20494.

Price, J.F., Weller, R.A., Pinkel, R., 1986. Diurnal cycling: Observations and models of the upper ocean response to diurnal heating, cooling, and wind mixing. Journal of Geophysical Research 91, 8411–8427.

Sarmiento, J.L., Hughes, T.M.C., Stouffer, R.J., Manabe, S., 1998. Simulated response of the ocean carbon cycle to anthropogenic climate warming. Nature 393, 245–249.

Sarmiento, J.L., Toggweiler, J.R., 1984. A new model for the role of the oceans in determining atmospheric pCO_2. Nature 308, 621–624.

Sjoberg, B., Stigebrandt, A., 1992. Computations of the geographical distribution of energy flux to mixing processes via internal tides and the associated vertical circulation of the ocean. Deep Sea Research 39, 269–291.

Takahashi, T., Olafsson, J., Goddard, J.G., Chipman, D.W., Sutherland, S.C., 1993. Seasonal variation of CO_2 and nutrients in the high-latitude surface oceans—A comparative study. Global Biogeochemical Cycles 7, 843–878.

Toggweiler, J.R., 1999. Variation of atmospheric CO_2 by ventilation of the ocean's deepest water. Paleoceanography 14, 571–588.

Toggweiler, J.R., Carson, S., 1995. What are upwelling systems contributing to the ocean's carbon and nutrient budgets? In: Summerhayes, C.P., Emeis, K.-C., Angel, M.V., Smith, R.L., Zeitschel, B. (Eds.), Upwelling in the Ocean: Modern processes and ancient records.. Wiley, New York, pp. 337–360.

Toggweiler, J.R., Samuels, B.L., 1993. New radiocarbon constraints on the upwelling of abyssal water to the ocean's surface.. In: Heimann, M. (Ed.), The Global Carbon Cycle.. Springer, New York, pp. 363–365.

Toggweiler, J.R., Samuels, B.L., 1998. On the ocean's large-scale circulation near the limit of no vertical mixing. Journal of Physical Oceanography 28, 1832–1852.

Toole, J.M., Polzin, K.L., Schmitt, R.W., 1994. Estimates of diapycnal mixing in the abyssal ocean. Science 264, 1120–1123.

Veronis, G., 1975. The role of models in tracer studies. In: Numerical Models of Ocean Circulation. National Academy Science, pp. 133–146.

Visbeck, M., Marshall, J., Haine, T., Spall, M., 1997. Specification of eddy transfer coefficients in coarse-resolution ocean circulation models. Journal of Physical Oceanography 27, 381–402.

Walker, S.J., Weiss, R.F., Salameh, P.K., 2000. Reconstructed histories of the annual mean atmospheric mole fractions for the halocarbons CFC-11, CFC-12, CFC-113, and carbon tetrachloride. Journal of Geophysical Research-Oceans, 14 285–14 296.

Whitehead, J.A., Worthington, L.V., 1982. The flux and mixing rates of Antarctic Bottom Water within the North Atlantic. Journal of Geophysical Research 87, 7903–7924.

Winton, M., Hallberg, R.W., Gnanadesikan, A., 1998. Simulation of density-driven frictional downslope flow in z-coordinate ocean models. Journal of Physical Oceanography 28, 2163–2174.

Worthington, L.V., 1977. The case for near-zero production of Antarctic Bottom Water. Geochimica et Cosmochimica Acta 41, 1001–1006.

Wunsch, C., Hu, D., Grant, B., 1983. Mass, salt, heat and nutrient fluxes in the South Pacific Ocean. Journal of Physical Oceanography 13, 725–753.

Yamanaka, Y., Tajika, E., 1996. The role of the vertical fluxes of particulate organic matter and calcite in the ocean carbon cycle: Studies using an ocean biogeochemical general circulation model. Global Biogeochemical Cycles 10, 361–382.